ABSTRACT

Title of Thesis: ENHANCED DIFFUSIOOSMOSIS AND THERMOOSMOSIS IN POLYELECTROLYTE-BRUSH-FUNCTIONALIZED NANOCHANNELS

Raja Sampath Maheedhara

Thesis directed by: Dr. Siddhartha Das
Department of Mechanical Engineering

One of the holy grails of nanofluidic systems is to ensure significant flow rates without applying a large pressure gradient. This has motivated researchers to study different mechanisms of liquid transport in nanochannels involving physical effects that exploit the large surface-to-volume ratio of such nanochannels. This thesis will focus on two highly efficient non-pressure-driven flow mechanisms in nanochannels functionalized by grafting the inner walls of nanochannels with end-charged polyelectrolyte (PE) brushes. We study two mechanisms to achieve flow augmentation: (i) ionic diffusioosmosis (IDO), triggered by the application of an external concentration gradient, and (ii) ionic thermoosmosis (ITO), triggered by a temperature gradient. We find a non-intuitive scenario where the flow in nanochannels can be significantly augmented by grafting the nanochannels with PE brushes. Given the difficulty in attaining a desirable flow strength in nanochannels, we anticipate that this thesis will serve as an important milestone in the area of nanofluidics.

ENHANCED DIFFUSIOOSMOSIS AND THERMOOSMOSIS IN POLYELECTROLYTE-BRUSH-FUNCTIONALIZED NANOCHANNELS

by

Raja Sampath Maheedhara

Thesis submitted to the Faculty of the Graduate School of the
University of Maryland, College Park in partial fulfillment
of the requirements for the degree of
Master of Science
2018

Advisory Committee:
Assistant Professor Siddhartha Das, Chair/Advisor
Associate Professor Amir Riaz
Assistant Professor Taylor Woehl

Acknowledgments

I would like to express my gratitude to my advisor, Dr. Siddhartha Das, who had kindly taken me as his student more than a year ago. His depth of insights on a host of topics in the field has inspired me to try and emulate the process of enjoying learning itself. I am also grateful to him for giving me the opportunity to work on or learn a wide variety of topics that are of immense importance in my professional career. Last but not the least, I am grateful for his friendly attitude and tolerance of my mistakes, which have been far too many to keep count of.

I am deeply indebted to my parents, who have kept up encouraging me to aim higher, despite their own financial and health-related hiccups. I can only hope to repay the smallest of the portions of that debt. I also want to thank my two loving sisters for being always there for me, come hell or high water.

Finally, I would like to express my thanks to my lab mates, Harnoor, Huoyan and Guang, without whom this work would have been incomplete.

Table of Contents

List of Figures

Chapter 1: Introduction

In this chapter, brief descriptions are first provided to describe the functionalization of nanochannels for polymer and polyelectrolyte (PE) brushes and the different applications in which such brush-functionalized nanochannels are used. Following that, the literature on liquid transport in such brush-grafted nanochannels are discussed. Subsequently, the key research questions that will be addressed in this thesis are discussed. Finally, the chapter ends with the outline of the structure and the organization of the thesis.

1.1 Polymer and polyelectrolyte brushes: Applications

When chains of polymer molecules are attached to a substrate densely enough, the interplay of the steric forces between the polymer molecules (in the form of the excluded volume interactions) and the entropic effects (in the form of intrachain elastic interactions) enforce the polymer molecules to attaion "brush"-like configuration, characterized by the height of the polymer brushes [1–11]. When these polymer brushes are charged, they are called polyelectrolyte (PE) brushes [12, 13]. In such a system, an additional electrostatic force of interaction among the brushes also contributes to the overall brush configuration. The presence of an electrolyte

around charged PE brush creates an additional force due to the interaction of the brushes with the induced electric double layer (EDL). The exact extent of this interaction depends on various parameters such as the such as the pH and salt content of the electrolyte, charge density on the brushes, monomer distribution along the brushes, possible confining effects where brushes are grafted on opposing surfaces, etc [14–21]. The characteristics of the PE brushes, i.e. the brush height, the brush grafting density, the charge density on the brushes, can thus be tuned as a response to the environmental stimuli, which in turn makes these brushes ideal candidates for functionalizing interfaces for a wide range of applications such as regulating cell adhesion and cell culture [22, 23], modifying the substrate wettability [24–26], targeted drug delivery [27, 28], enhanced oil recovery [29], stabilizing emulsions [30], designing nanocomposites with tunable properties [31], flow valving [32, 33], ion sensing and manipulation [34–36], biosensing [37, 38], current rectification [39], fabrication of nanofluidic diodes [40, 41], and many more.

1.2 Liquid flows in polymer and PE brush grafted nanochannels

In comparison to the analysis of ion transport, liquid flows in nanochannels functionalized with the grafting of PE brushes have been significantly less studied. This has been primarily due to the well-accepted understanding that the presence of the brushes will invariably retard the liquid transport in such brush-grafted nanochannels stemming from the significantly large drag force imparted by the brushes. In fact, most of the existing studies on liquid transport in PE-brush-grafted nanochannels

confirm this message [19, 33, 42–48]. These papers suffer from one key limitation: while modelling the transport that often depends on the salt concentration of the electrolyte, they invariably consider a brush height that is unaffected by the salt and pH effects. In a recent paper, Chen and Das [49] corrected this theoretical lacuna and probed the electroosmotic (EOS) transport in a nanochannel grafted with end-charged PE brushes in a setting that accounted for the appropriate salt-dependent brush configuration. More importantly they discovered a most remarkable fluid mechanical situation in the context of liquid transport in brush grafted nanochannels: they witnessed that for end-charged less densely grafted brushes, the localization of EDL at the brush tip (this localization becomes stronger at larger salt concentration) and the effect of the resulting localization of the EOS body force (arising from the interaction of the EDL charge density and the applied axial electric field) became so severe that the influence of the brush-induced enhanced drag was overwhelmed and one witnessed an EOS transport that was more augmented as compared to the EOS transport in brush-free nanochannels. Of course, for densely grafted end-charged brushes, the drag force was again found to be larger making the overall EOS transport weaker in comparison to the EOS transport in brush-free nanochannels. In this thesis, we attempt to build on their work and apply this modeling in the context of an induced EOS transport in presence of an applied concentration/temperature gradient, i.e., investigate for the first time the ionic diffusioosmosis and ionic thermoosmosis in end-charged PE-brush-grafted nanochannels.

1.3 Main agenda of the present thesis

Our work aims to provide a theoretical basis for the augmentation/reduction of liquid flows in nanochannels with an applied concentration gradient (Diffusio-osmosis) and thermal gradient (Thermo-osmosis) across the channel.

Ionic diffusio-osmosis refers to the induction of a flow field and a tangential electric field in an electrolyte confined in a nano-channel in the presence of an applied gradient of the solvent concentration. We consider a case where the length of the nanochannel is small enough such that the concentration profile can be treated as linear along the length of the channel. In such a system, when there is an applied charge density on the walls, an electric double layer (EDL) is formed. This EDL plays an important role in creating an imbalance in the number density of the cations and anions of the electrolyte in the bulk liquid. Such an imbalance, combined with the linearly varying profile of the concentration, then triggers a Fickian diffusion of the electrolyte, thus inducing a flow in the bulk liquid. It is important to note here that this effect is negligible in a macro-channel, as the double layer is diminutive in comparison to the channel width. However, such effects become important at micro and nano scales. This induced flow creates a charge separation due to the difference in the diffusivity of the ions, and combined with the electric field due to the EDL, leads to a net electric field, which in turn drives the flow. This, as we will present in the later chapters, leads to a two way coupling between the induced electric field and the induced flow field. While the induced electric field is mostly dominated by the gradient in the number density and not as much by the induced flow field, this

study provides an insight into the factors influencing the strength and direction of the induced flow.

On the other hand, Ionic thermo-osmosis occurs when a temperature gradient is applied across a channel filled with an electrolyte. This temperature gradient has two significant effects: (i) It creates a gradient in the number concentrations of the ions, which creates an effect similar to ionic diffusio-osmosis, and (ii) It provokes differential response between the positive and negative ions in case of a difference in their heats of transport. Similar to ionic diffusio-osmosis, thus, this leads to an osmotic flow, which is two-way coupled with the induced electric field. In both these phenomena, the induced flow field is found to be significantly affected when the channels are functionalized with PE-brushes. In this study, we will look at some of the factors that affect this flow: (i) factors that are characteristics of the brushes viz., the length of the brushes, and (ii) factors relating to the electrolyte, viz., salt concentration and diffusivity ratios. We find that the interplay of these factors determine to what extent the flow is either augmented or reduced. This, we believe, would be highly useful in understanding the physics of the flow augmentation, and in exploring related avenues for the same.

1.4 Organization of the thesis

Chapter 2 of this thesis deals with the effect of the ionic diffusioosmosis in the presence of an axial salt concentration gradient in a nanochannel filled with an electrolyte solution and grafted with end-charged PE brushes. We elucidate the

importance of such a system based on past studies. Building on the past efforts on the modeling of EDL electrostatics and brush interaction - both among the PE brushes and between the PE brushes and the fluid - we then, provide the theoretical foundation for the underlying physics in the problem. Following a brief explanation of the solution techniques used, we then provide some interesting results of the parametric studies, the parameters being concentration of the electrolyte itself, the length of each PE brush, and the effect of a skewed diffusivities between the cations and the anions of the electrolyte. We document the differences in the results , and attempt to provide a physical explanation for the differences.

Chapter 3 of this thesis deals with the effect of the ionic diffusioosmosis in the presence of an axial temperature concentration gradient in a nanochannel filled with an electrolyte solution and grafted with end-charged PE brushes. The importance of such a system lies in the fact that in many situations, the application of a termperature gradient is easier than the application of a concentration gradient. Following the template of chapter 2, we provide the theoretical foundation of the brush physics and the physics of the interaction of the brushes with the electrolyte. We then provide parametric results for the induced flow field and the induced electric field. The parameters we have considered in this chapter include the concentration of the electrolyte, the diffusivity ratio of the cations to anions, the difference in heats of transport between the cations and the anions, and finally, the brush parameters. Both the chapters end in a presentation of the summary of our findings, and scope of future work.

Chapter 2: Ionic Diffusoosmosis in Nanochannels Grafted with End-charged Polyelectrolyte Brushes

In this chapter[1]*, we develop a theory to study the imposed axial salt-concentration-gradient-driven ionic diffusioosmosis (IDO) in soft nanochannels or nanochannels grafted with end-charged poly- electrolyte (PE) brushes. Our analysis first quantifies the diffusioosmotically induced electric field, which is primarily dictated by the imposed concentration gradient (CG) with little contribution of the induced osmosis. This induced electric field triggers an electroosmotic (EOS) transport, while the net diffusioosmotic (DOS) transport results from a combination of this EOS transport and a chemiosmotic (COS) transport arising from the pressure gradient induced by the applied CG. Our results unravel that the DOS transport is massively enhanced in nanochannels grafted with PE brushes with weak grafting density stemming from the significantly enhanced EOS transport caused by the localization of the EOS body force away from the nanochannel walls. This augmentation is even stronger for cases where the COS transport aids the EOS transport. On the other hand, the DOS transport gets*

[1]Contents of this chapter have been submitted as: *R. S. Maheedhara, H. S. Sachar, H. Jing, and S. Das,"Ionic Diffusoosmosis in Nanochannels Grafted with End-charged Polyelectrolyte Brushes," J. Phys. Chem. B (accepted).*

severely reduced in nanochannels grafted with dense PE brushes owing to the severity of the brush-induced additional drag force. We anticipate that these findings will help to unravel an entirely new understanding of induced electrokinetic transport in soft nanochannels.

2.1 Introduction

Grafting nanoscale solid-liquid interfaces (e.g., surfaces of metallic nanoparticles or the inner walls of nanochannels) by charged polyelectrolyte (PE) brushes have been extensively used for a myriad of applications ranging from targeted drug delivery [50–52], oil recovery [53], water harvesting [54], selective sensing of ions and charged biomolecules [36,55–57], gating and current rectification [35,39,58], and many more. These applications depend on the functionalities rendered to these interfaces by such PE grafting and have been quantified in terms of the responses of these brushes to the substance-specific cues or some specific environmental cues. For such examples, often only the thermodynamics and the electrostatics of these brushes have been theoretically probed [1–3, 5–7, 9, 14, 15]. On the other hand, relatively less research has been conducted for probing the detailed fluid physics at these PE-brush-grafted nanoscale interfaces. More significantly, the existing studies invariably neglect the role of thermodynamics (e.g., coupled description of brush configuration and brush electrostatics) in the fluid mechanics description [42, 43, 45, 59–67]. This becomes evident from the fact that these papers invariably consider a constant, ion-concentration-independent brush height while modelling fluid flow at the brush-grafted interfaces.

Very recently Chen and Das addressed this limitation and provided possibly the first theoretical model where the PE brush thermodynamics has been accounted for in the description of the flow field in nanochannels grafted with such PE brushes [49]. In this paper, electroosmotic (EOS) transport through the nanochannels grafted with end-charged PE brushes (such interfaces designed with end-charged PE brushes have been considered previously as well [19, 68, 69]) was investigated – the fluid mechanics model indeed accounted for the correct thermodynamics and the electrostatic behavior of these end-charged brushes [49]. More importantly, this study established that the presence of significantly tall brushes with weak grafting density will actually augment the EOS transport in brush-grafted nanochannels in comparison to the brush-free nanochannels. This was an extremely counter-intuitive finding given the fact that the presence of the brushes has always been believed to retard the nanofluidic transport on account of the additional brush-induced drag [33]. This highly non-intuitive phenomenon was explained by noting that the end-charged brushes localized the EDL and hence the EDL-induced EOS body force at the non-grafted end of the brushes, which is significantly away from the wall (the location of the maximum drag force). As a consequence, the EOS body force of a given strength will have a much larger effect on the velocity field triggering a much augmented velocity field. For large salt concentrations, the EDLs became thin and consequently, this effect of the localization of the EOS body force away from the wall became even more prominent leading to a larger strength of the EOS transport. Of course, for the PE brushes having a much larger grafting density, the brush-induced drag force outweighed this effect associated with the localization of the EDL charge density and hence one indeed witnessed the

classical result where the presence of the brushes severely weakened the flow field.

In the present paper, we shall study the ionic diffusioosmosis (IDO) in such nanochannels grafted with end-charged PE brushes. Diffusioosmosis refers to the liquid transport in presence of an applied gradient in concentration in ions or nonionic solute – this gradient triggers a driving force (in form of pressure gradient and/or an electric field) that triggers the fluid motion [70–74]. There has been signifiant effort in fundamentally understanding the DO in presence of both ionic [70, 74–85] and non-ionic solute gradients [73, 86–93] and applying that knowledge for a host of applications such as driving liquid flows in microchannels [88], amplifying the strength of interfacial flows [91], designing self-powered microdevices for sensing purposes [93], photo-induced manipulation of particles at solid-liquid interfaces [94], strategizing new methods for phase separations [95], and many more. In this paper, we study for the first time this new electrokinetic problem for soft nanochannels (i.e., nanochannels grafted with end-charged PE brushes). Our theory accounts for the thermodynamics and electrostatics of the brushes in developing the fluid mechanics model for the IDO in brush-grafted nanochannels. Our theory leads us to an integro-differential equation that is solved numerically to unravel the physics of the IDO. Firstly, we quantify the diffusioosmotically induced electric field, establishing the manner in which the imposed concentration gradient (CG) dictates this electric field with insignificant contribution from the induced osmotic effect. Secondly the diffusioosmotic (DOS) flow is described as a combination of the induced electroosmotic (EOS) transport (caused by this induced electric field) and a chemisoosmotic (COS) transport caused by the induced pressure gradient owing to this imposed CG. We compare the re-

sults of the PE-brush-grafted nanochannels with that of the brush-free nanochannels. While there is a less difference in the overall induced electric field between these two systems by virtue of the fact that the electric field is primarily dictated by the effect of the imposed CG, the velocity fields vary massively between the brush-free and brush-grafted nanochannels. The influence of charge localization induced enhancement of the EOS velocity field [49] ensures that for sufficiently long but weakly grafted brushes, the induced EOS transport and consequently the resulting DOS transport gets massively enhanced for the nanochannels grafted with the PE brushes. Furthermore, for conditions where the COS transport augments the EOS transport, this enhancement is even larger. Moreover, such dominant role of the EDL (and hence EOS body force) localization effect leads to a concentration-dependent behavior of the DOS flow field in brush-grafted nanochannels that is completely opposite to what occurs in brush-free nanochannels. Finally, we study the case where the grafting density of the brushes is much larger and therefore, on account of the dominant influence of the brush-induced drag force, the DOS transport gets severely reduced as compared to the DOS transport in brush-free nanochannels. In summary, our paper studies for the first time the electrokinetic problem of IDO in brush-grafted soft nanochannels unraveling fluid physics that can be instrumental for novel flow based applications involving functionalized, soft nanochannels.

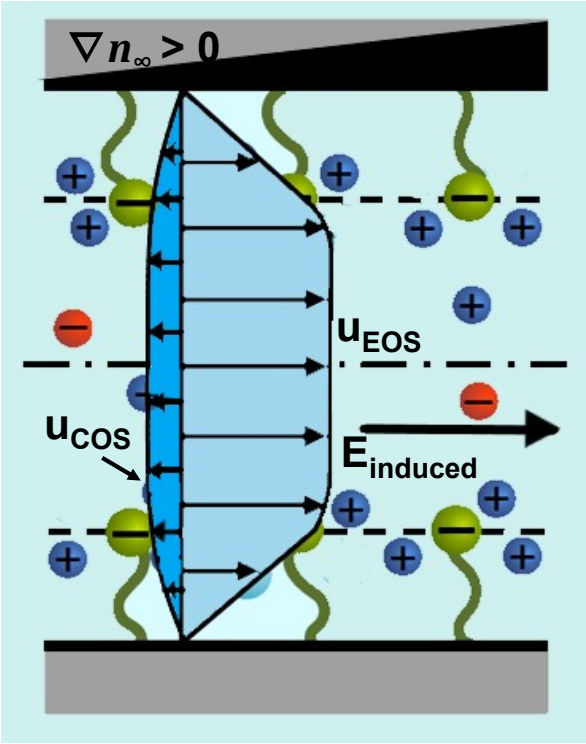

Figure 2.1: Schematic showing DOS transport in nanochannels grafted with end-charged brushes. The DOS flow is a combination of the EOS (caused by the induced electric field) and the COS flows, as illustrated in the schematic. The schematic shown here corresponds to non-negative values of the dimensionless diffusivity difference β.

2.2 Theory

We consider a nanochannel of half height h and length L grafted with end-charged PE brushes (see Fig. 1). The nanochannel is connected to bulk microfluidic reservoirs. We have previously studied the electrostatics, thermodynamics, ionic current, and electrokinetic transport in such nanochannels [19, 49, 69]. The calculation of the electrokinetic transport in these papers [49] is unique in the sense that it accounts for the appropriate coupling of the brush configuration and the resulting EDL electrostatics while computing the electrokinetic fluid flow. In the present paper, we would use this information on the coupled brush configuration and the resulting EDL electrostatics in order to quantify the ionic DOS transport. The IDO is triggered by imposing a constant axial ionic concentration gradient of strength $\nabla n_\infty = dn_\infty/dx$, such that $L\nabla n_\infty/n_\infty(x = 0)$ (here n_∞ is the bulk number density of the electrolyte ions or the electrolyte ion concentration in the microfluidic reservoirs). We shall first provide the coupled equilibrium description of the configuration of the end-charged PE brush and the induced EDL electrostatics. This description has already been provided in our previous paper [49] – we repeat it here for the sake of completion. Next, we shall use this equilibrium description to quantify the electric field induced due to the diffusioosmotic effect and the resulting nanofluidic velocity field (occurring due to the combined influence of the induced EOS and the COS velocities).

2.2.1 Equilibrium thermodynamics and electrostatics of the end-charged brushes

The equilibrium behavior of the end-charged brushes is obtained by minimizing the total free energy F of the brushes and the surrounding electrolyte:

$$F = F_{B,els} + F_{B,EV} + F_{B,elec} + F_{EDL}, \tag{2.1}$$

where $F_{B,els}$, $F_{B,EV}$ and $F_{B,elec}$ are the elastic, excluded volume, and electrostatic free energies associated with the brushes and F_{EDL} is the free energy associated with the induced EDL. These individual free energies can be expressed as:

$$\frac{F_{B,els}}{k_BT} = \frac{3d^2}{2N_pa_k^2}, \tag{2.2}$$

$$\frac{F_{B,EV}}{k_BT} = \frac{\omega N_p^2\sigma}{d}, \tag{2.3}$$

$$F_{B,elec} = \frac{\psi_s\sigma_{ch}}{\sigma}, \tag{2.4}$$

$$F_{EDL} = \frac{1}{\sigma}\int_{-h}^{0} f_{EDL}dy. \tag{2.5}$$

In the above equations, d is the brush height, N_p is the polymer size (or the number of monomers in the polymer chain), a_k is the Kuhn's length, $\omega = \frac{1-2\chi}{2}a_k^3$ (where χ is the Flory exponent), ψ_s is the electrostatic potential at the non-grafted charged end of the brushes, σ_{ch} is the constant (pH-independent) charge density of the ends of the PE brushes, σ is the grafting density, and k_BT is the thermal energy. Finally, f_{EDL} is the density of the EDL energy and can be expressed as:

$$f_{EDL} = -\frac{\epsilon_0\epsilon_r}{2}|\frac{d\psi}{dy}|^2 + e\psi\left(n_+ - n_-\right) + k_BT\left[n_+\left(\ln\left(\frac{n_+}{n_\infty}\right)-1\right) + n_-\left(\ln\left(\frac{n_-}{n_\infty}\right)-1\right)\right], \tag{2.6}$$

where ϵ_0 is the permittivity of free space, ϵ_r is the relative permittivity of water, ψ is the electrostatic potential, $n_\pm$ is the number density of the symmetric monovalent electrolyte ions, and n_∞ is the bulk number density of the ions.

The final free energy equation obtained by using eqs.(2-6) in eq.(1) is minimized to obtain the equilibrium conditions. The minimization with respect to ψ yields the Poisson equation:

$$\frac{d^2\psi}{dy^2} = -\frac{e\left(n_+ - n_-\right)}{\epsilon_0\epsilon_r}. \tag{2.7}$$

On the other hand, the minimization of this free energy equation with respect to $n_\pm$ leads to the well-known Boltzmann distribution:

$$n_\pm = n_\infty \exp\left(\mp\frac{e\psi}{k_B T}\right). \tag{2.8}$$

Finally the minimization of the free energy equation with respect to ψ_s yields the boundary condition at the location of the brush tip (i.e., $y = -h+d$) for the nanochannel bottom half (see Chen and Das [49] for detailed derivation):

$$\left(\frac{d\psi}{dy}\right)_{y=(-h+d)^+} - \left(\frac{d\psi}{dy}\right)_{y=(-h+d)^-} = -\frac{\sigma_{ch}}{\epsilon_0\epsilon_r}, \tag{2.9}$$

where d is the equilibrium brush height. The Poisson-Boltzmann equation, obtained by using eq.(2.8) to replace $n_\pm$ in terms of ψ in eq.(2.7), is solved numerically in presence of the boundary condition expressed in eq.(2.9) as well as the conditions expressed below:

$$\left(\frac{d\psi}{dy}\right)_{y=-h} = 0, \quad \left(\frac{d\psi}{dy}\right)_{y=0} = 0, \quad (\psi)_{(y=-h+d)^+} = (\psi)_{(y=-h+d)^-}. \tag{2.10}$$

Once the equilibrium ψ and $n_\pm$ distribution have been obtained, we use it in eqs.(5,6) to compute the equilibrium value of F_{EDL}. Of course, this equilibrium F_{EDL} will

depend on the brush height d. This equilibrium F_{EDL} is used in the overall free energy, which is then minimized with respect to d numerically to obtain the equilibrium brush height (i.e., equilibrium value of d). This is the same procedure that we have used in our previous papers [19, 49].

2.2.2 Diffusioosmotically Induced Electric Field

In order to obtain the diffusioosmotically induced electric field, we need to equate the net current in the system to zero, which is identical to making the integral of the difference between the cationic and anionic fluxes to zero, i.e.,

$$\int_{-h}^{h} (J_+ - J_-)\, dy = 0, \tag{2.11}$$

where the fluxes ($J_\pm$) can be expressed as:

$$J_\pm = -D_\pm \left[\nabla n_\pm \pm \frac{e}{k_B T} n_\pm (\nabla\psi - E)\right] + n_\pm u. \tag{2.12}$$

In the above equation, $D_\pm$ are the diffusivities of cations and anions, u is the induced velocity field (a combination of the EOS and COS velocity fields) and E is the induced electric field. Using eq.(3.2) in eq.(3.1), we shall eventually get the dimensionless diffusioosmotically induced electric field (please see the Appendix for detailed derivation):

$$\begin{aligned}\bar{E} = \frac{E}{E_0} =& Pe \frac{\int_{-1}^{1} 4\bar{u}\sinh(\bar{\psi}) d\bar{y}}{\int_{-1}^{1} \left[(1+\beta_1)\, e^{-\bar{\psi}} + (1-\beta_1)\, e^{\bar{\psi}}\right] d\bar{y}} + \\ & \frac{\int_{-1}^{1} \left\{\bar{n}_1' \left[(1+\beta)\, e^{-\bar{\psi}} - (1-\beta)\, e^{\bar{\psi}}\right]\right\} d\bar{y}}{\int_{-1}^{1} \left\{\left[(1+\beta)\, e^{-\bar{\psi}} + (1-\beta)\, e^{\bar{\psi}}\right]\right\} d\bar{y}},\end{aligned} \tag{2.13}$$

where $\bar{y} = y/h$, $E_0 = k_B T/(eL)$, $\bar{u} = u/U^*$ (where U^* is the characteristic velocity scale that defines the Peclet number: $Pe = U^* L/(D_+ + D_-)$), $\bar{\psi} = e\psi/(k_B T)$, $\beta = \frac{D_+ - D_-}{D_+ + D_-}$, and $\bar{n}_1' = \frac{L\nabla n_\infty}{n_\infty}$.

2.2.3 Diffusioosmotic (DOS) Velocity Field

In order to obtain the DOS velocity field, we shall employ the Navier-Stokes (NS) equation. The NS equation in y-direction yields the necessary pressure field, i.e.,

$$\frac{\partial p}{\partial y} + 2e\left(n_+ - n_-\right)\frac{d\psi}{dy} = 0$$

$$\Rightarrow \partial p = 2k_B T n_\infty \sinh\left(\bar{\psi}\right) d\bar{\psi} \Rightarrow p = p_{atm} + 2k_B T n_\infty \left[\cosh\left(\bar{\psi}\right) - 1\right]. \tag{2.14}$$

Finally, the NS equation in the x-direction yields (considering only the nanochannel bottom half):

$$\begin{aligned} \eta\frac{d^2u}{dy^2} &= \frac{\partial p}{\partial x} + \eta\frac{u}{k_d} - e\left(n_+ - n_-\right)\left(E - \nabla\psi\right) \quad for \ -h \le y \le -h + d, \\ \eta\frac{d^2u}{dy^2} &= \frac{\partial p}{\partial x} - e\left(n_+ - n_-\right)\left(E - \nabla\psi\right) \quad for \ -h + d \le y \le 0. \end{aligned} \tag{2.15}$$

Eq.(3.6) can be expressed in dimensionless form as (see the Appendix for the detailed derivation):

$$\frac{d^2\bar{u}}{d\bar{y}^2} = A\left\{\bar{n}_1'\left[\cosh\left(\bar{\psi}\right)-1\right]\right\} + \alpha^2\bar{u} + A\sinh\left(\bar{\psi}\right)\left\{Pe\frac{\int_{-1}^{1}4\bar{u}\sinh\left(\bar{\psi}\right)dy}{\int_{-1}^{1}\left[\left(1+\beta\right)e^{-\bar{\psi}}+\left(1-\beta\right)e^{\bar{\psi}}\right]d\bar{y}} + \frac{\int_{-1}^{1}\bar{n}_1'\left[\left(1+\beta\right)e^{-\bar{\psi}}-\left(1-\beta\right)e^{\bar{\psi}}\right]d\bar{y}}{\int_{-1}^{1}\left[\left(1+\beta\right)e^{-\bar{\psi}}+\left(1-\beta\right)e^{\bar{\psi}}\right]d\bar{y}}\right\}$$
$$for\ \ -1 \le \bar{y} \le -1+\bar{d},$$
$$\frac{d^2\bar{u}}{d\bar{y}^2} = A\left\{\bar{n}_1'\left[\cosh\left(\bar{\psi}\right)-1\right]\right\} + A\sinh\left(\bar{\psi}\right)\left\{Pe\frac{\int_{-1}^{1}4\bar{u}\sinh\left(\bar{\psi}\right)dy}{\int_{-1}^{1}\left[\left(1+\beta\right)e^{-\bar{\psi}}+\left(1-\beta\right)e^{\bar{\psi}}\right]d\bar{y}} + \frac{\int_{-1}^{1}\bar{n}_1'\left[\left(1+\beta\right)e^{-\bar{\psi}}-\left(1-\beta\right)e^{\bar{\psi}}\right]d\bar{y}}{\int_{-1}^{1}\left[\left(1+\beta\right)e^{-\bar{\psi}}+\left(1-\beta\right)e^{\bar{\psi}}\right]d\bar{y}}\right\}$$
$$for\ \ -1+\bar{d} \le \bar{y} \le 0, \tag{2.16}$$

where $\bar{d} = d/h$, η is the dynamic viscosity, $A = \frac{2k_BTn_\infty}{L}\frac{h^2}{\eta U^*} = \frac{\Pi_{osm}}{\Pi_{drive}}$, and $\alpha = h^2/k_d$ [where $k_d = a_k^2\left(\frac{d}{\sigma a_k^3 N_p \phi}\right)^2$ is the permeability, with ϕ being the monomer distribution along the length of the PE brush]. It is obvious that we arrive at eq.(3.6) by using the expression of E [see eq.(2.13)]. Eq.(3.6) is an integro-differential equation in $\bar{u}$, which is solved numerically in presence of the boundary conditions expressed below.

$$\left(\bar{u}\right)_{\bar{y}=-1} = 0,\ \ \left(\bar{u}\right)_{\bar{y}=(-1+\bar{d})^+} = \left(\bar{u}\right)_{\bar{y}=(-1+\bar{d})^-},\ \ \left(\frac{d\bar{u}}{d\bar{y}}\right)_{\bar{y}=(-1+\bar{d})^+} = \left(\frac{d\bar{u}}{d\bar{y}}\right)_{\bar{y}=(-1+\bar{d})^-},\ \ \left(\frac{d\bar{u}}{d\bar{y}}\right)_{\bar{y}=0} = 0. \tag{2.17}$$

Subsequently, this $\bar{u}$ is used to obtain the dimensionless electric field $\bar{E}$ [see eq.(2.13)]. Obviously, both the solution for $\bar{u}$ and $\bar{E}$ will depend on $\bar{\psi}$ – section IIA provides a method to calculate $\bar{\psi}$.

2.3 Results and Discussions

2.3.1 Variation of the EDL electrostatic field ψ

Fig. 2 provides the variation of the dimesnionless EDL electrostatic field ψ for nanochannels with and without the grafted PE brushes for different values of bulk salt concentration. We ensure that the charge density of the non-grafted ends of the end-charged brushes is identical to the charge density of the inner walls of the brush-free nanochannels. In our previous paper, we have presented the results for the ψ variation for nanochannels grafted with end-charged PE brushes [49]. We repeat them here for the sake of continuity and for the better understanding of the diffusioosmotic phenomena. For the nanochannel without the brushes the location for the $|\bar{\psi}|_{max}$ is at the nanochannel walls, given the fact that the nanochannel walls are charged [see Fig. 2(a)]. This changes for the nanochannels grafted with the end-charged PE brushes. For these brushes the charges are localized at their non-grafted ends and as a consequence, one witnesses the attainment of $|\bar{\psi}|_{max}$ at the location of these ends, i.e., significantly away from the nanochannel walls. Smaller ℓ or larger grafting density leads to a larger equilibrium brush height – as a consequence, we witness the attainment of $|\bar{\psi}|_{max}$ at a location that is further away from the nanochannel wall for $\ell = 22\ nm$ [see Fig. 2(c)] as compared to $\ell = 80\ nm$ [see Fig. 2(a)]. Furthermore, regardless of the presence or the absence of the PE brush grafting, one witnesses a larger $|\bar{\psi}|$ at any transverse location for a smaller salt concentration (c_∞). Smaller c_∞ implies a larger value of the EDL thickness λ – therefore, given the fact that

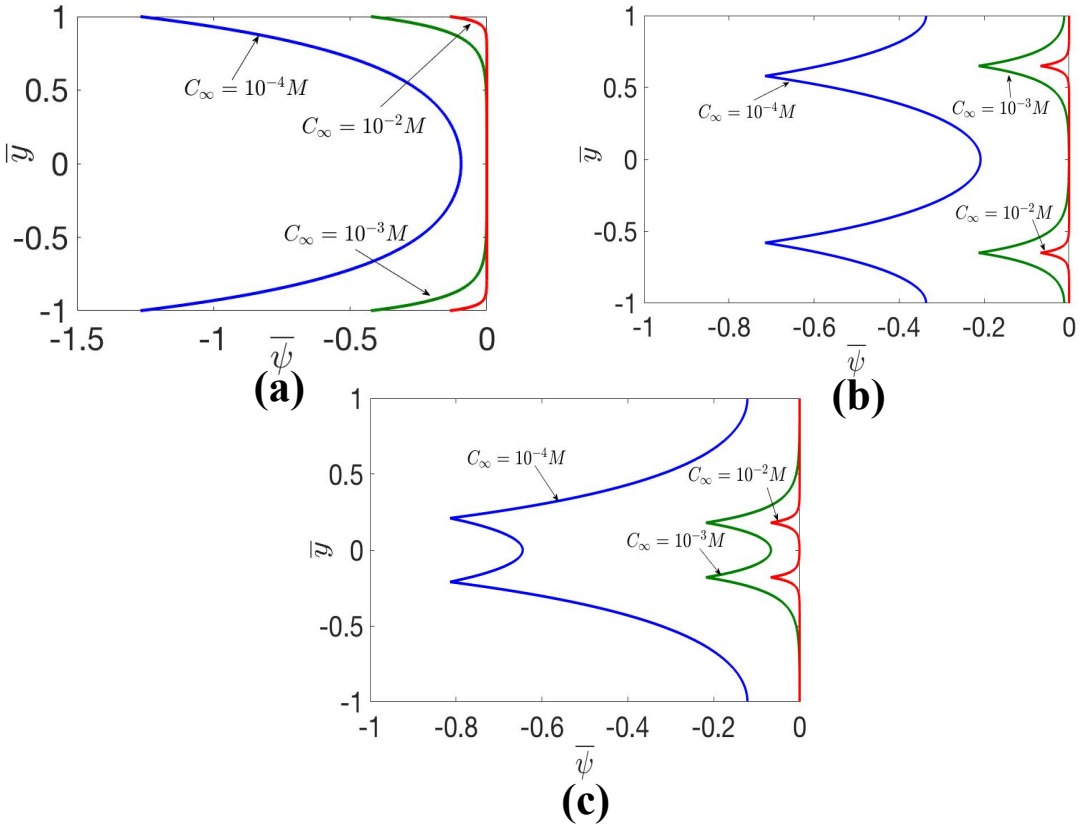

Figure 2.2: Transverse variation of $\bar{\psi}$ for (a) brush-free nanochannels, (b) nanochannels grafted with PE brushes with large grafting density (with $\ell = 88\,nm$, $N_p = 2000$), and (c) nanochannels grafted with PE brushes with weak grafting density (with $\ell = 22\ nm$, $N_p = 2000$). Results are shown for three different bulk salt concentrations, namely $c_\infty = 10^{-4}\ M,\ 10^{-3}\ M,\ 10^{-2}\ M$ for each of (a-c). Other parameters are $\sigma_{ch} = -0.0008 C/m^2$ (this charge density is the charge density for brush-free nanochannel walls and the ends of the end-charged PE brushes for nanochannels with PE brushes), $h = 100nm$, $\chi = 0.4$, $a_k = 1nm$, $k_B = 1.38 \times 10^{-23}\ J/K$, $T = 300\ K$, $e = 1.6 \times 10^{-19} C$, $\epsilon_0 = 8.8 \times 10^{-12} F/m$. These figures are adapted with permission from Ref [49], Copyright (2017) American Chemical Society.

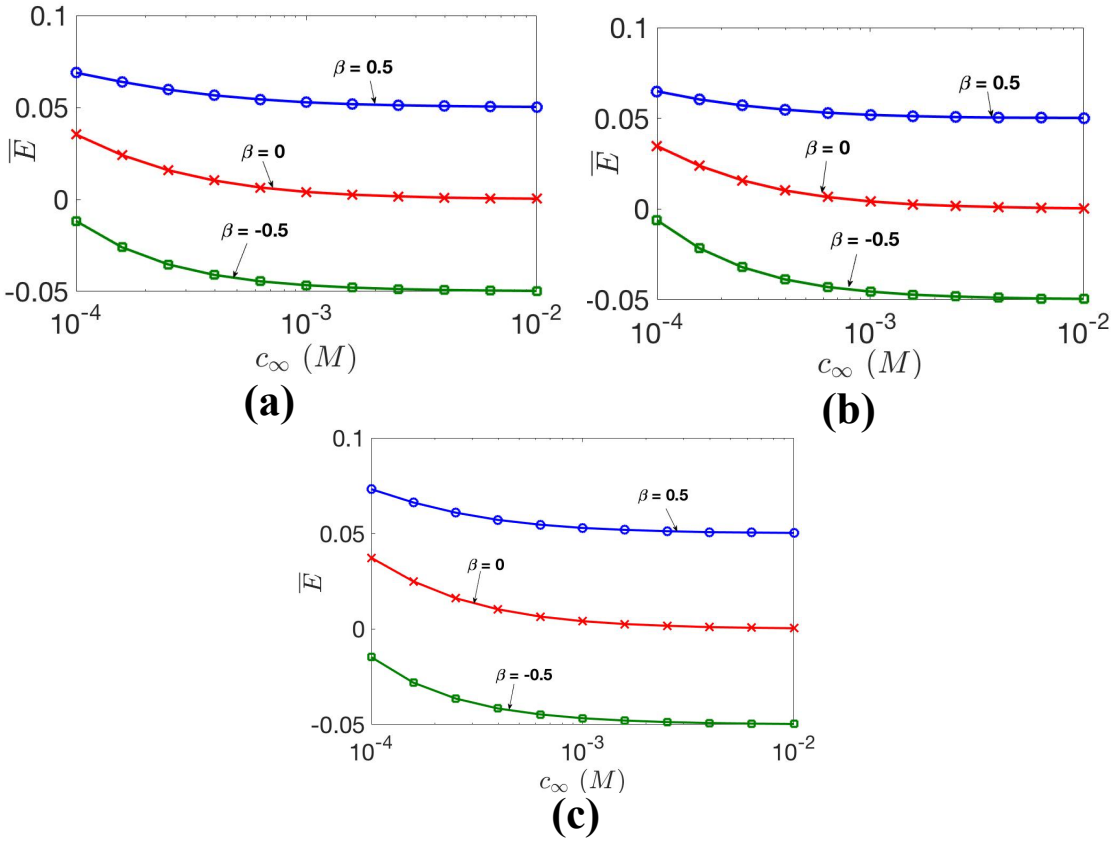

Figure 2.3: Variation of the diffusioosmotically induced electric field (expressed in dimensionless form) with bulk salt concentrations for (a) brush-free nanochannels, (b) nanochannels grafted with PE brushes with large grafting density (with $\ell = 88\ nm$, $N_p = 2000$), and (c) nanochannels grafted with PE brushes with weak grafting density (with $\ell = 22\ nm$, $N_p = 2000$).. Results are shown for three different values of β for each of (a-c). We consider $L\frac{\nabla n_\infty}{n_\infty} = 0.1$, while the other parameters are identical to those used in Fig. 2.

$|\bar{\psi}| \propto \lambda\sigma_{ch}$, one should witness a larger $|\bar{\psi}|$ for a given σ_{ch}. These information on the variation on $\bar{\psi}$ will help us to better explain the different DOS behaviors.

2.3.2 Variation of the diffusioosmotically induced electric field

Fig. 3 shows the variation of the dimensionless diffusioosmotically induced electric field for the nanochannels with and without the brushes as a function of salt concentration and β. The electric field is a combination of the osmotic effects (implying the electric field caused by the downstream advective migration of the charge imbalance present within the EDL) (please see the first term on the right hand side in eq. 13) and the imposed concentration gradient (CG) effect (please see the second term on the right hand side in eq. 13). The osmotic contribution is relatively weak in comparison to that due to the CG effect. The exact extent of the relative contribution of this osmotic component, as will be discussed later, depends on the presence (and the grafting density) of the brushes as well as the salt concentration. On the other hand, the contribution of the imposed CG effect on the induced electric field is contributed both by the diffusivity difference between the cations and anions (dictated by the parameter β) and the very fact that there is a charge imbalance induced by the EDL. For $\beta = 0, 0.5, -0.5$, this CG-imposed contribution of the electric field can be obtained as (considering small $|\bar{\psi}|$ and therefore using DH approximation in eq. 13, i.e., expressing $e^{\pm\bar{\psi}} = 1 \pm \bar{\psi}$):

$$\left(\bar{E}\right)_{CG,\beta=0} = -\frac{\bar{n}_1'}{2}\int_{-1}^{1}\bar{\psi}d\bar{y}, \quad \left(\bar{E}\right)_{CG,\beta=0.5} = \bar{n}_1'\frac{\int_{-1}^{1}(1-\bar{\psi})d\bar{y}}{\int_{-1}^{1}(2-\bar{\psi})d\bar{y}},$$
$$\left(\bar{E}\right)_{CG,\beta=-0.5} = -\bar{n}_1'\frac{\int_{-1}^{1}(1+2\bar{\psi})d\bar{y}}{\int_{-1}^{1}(2+\bar{\psi})d\bar{y}}. \tag{2.18}$$

$\bar{\psi}$ is always negative and $\bar{n}_1'$ is always positive. Accordingly, from eq.(18), we can easily identify why for $\beta = 0$ one witnesses a positive electric field for both brush-free and brush-grafted nanochannels (see Fig. 3). On the other hand, for $\beta > 0$, a negative $\bar{\psi}$ would imply an even larger positive value of E for both brush-free and brush-grafted nanochannels (see Fig. 3). This effect of $\beta > 0$ can be understood by noting the fact that a larger mobility of the counterions (which corresponds to a positive β) augments the effect associated with the charge difference of the EDL. Smaller c_∞ leads to a larger magnitude of $|\bar{\psi}|$. Accordingly for both $\beta = 0$ and $\beta = 0.5$, the positive value of E will be larger for smaller c_∞ for both brush-free and brush-grafted nanochannels (see Fig. 3). Completely contrary to these behaviors is the case corresponding to $\beta = -0.5$. This refers to a situation where the coions have higher mobilities, which in turn will nullify the effect associated with the EDL electrostatic potential. Accordingly for weak enough value of $|\bar{\psi}|$ the electric field can indeed be negative (see eq. 18) and this negative magnitude is enhanced for weaker $|\bar{\psi}|$ values. This also justifies a weaker negative magnitude of ψ for smaller c_∞ that corresponds to a larger magnitude of $|\bar{\psi}|$. This is true for both nanochannels with and without grafted PE brushes. We next consider the influence of the osmotic component of the electric field. For the same DH consideration, we can use eq.(13) to show that this component is proportional to $\bar{u}\bar{\psi}$, i.e., proportional to the effects of advection of the EDL charge density. For the case of very densely grafted PE brushes, the significantly small velocity component (as evident in Fig. 6 later) would lead to a very weak contribution of the osmotic effect and accordingly, as yielded by our analysis (results not shown here) the DOS electric field is effectively the electric field due to the

imposed CG. On the other hand, for cases of brush free nanochannels or nanochannels grafted with PE brushes with weak grafting density, the velocity field is significantly higher ensuring a finite (albeit less than 20%, as revealed by our analysis) variation of the overall electric field. However, this finite osmotic contribution mostly occurs for smaller salt concentration that yields a much larger value of $\bar{\psi}$ (see Fig. 2). Finally, for the situations where the osmotic component has insignificant contribution to the overall electric field (namely for the case of nanochannels grafted with PE brushes with large grafting density or nanochannels with or without brushes operating at large salt concentration), we witness insignificant effect of the presence of brushes on the overall value of E for a given β and c_∞. For such cases where the effect of the imposed CG dominates, the electric field is solely dictated by the integral of $\bar{\psi}$ across the channel height. This integral is proportional to the net surface charge density (at either the walls of the brush-free nanochannels or the non-grafted ends of the end-charged brushes decorating the nanochannel walls). This charge density being same for both brush free and brush-grafted nanochannels, we witness this nearly same E for a given c_∞ and a given β for both brush-free and brush-grafted nanochannels.

2.3.3 Variation of the diffusioosmotic (DOS) velocity field

Case of brush-free nanochannels:

In Fig. 4, we show the variation of the diffusioosmotically induced velocity field. This velocity field is a combination of the EOS velocity and the COS velocity fields. The

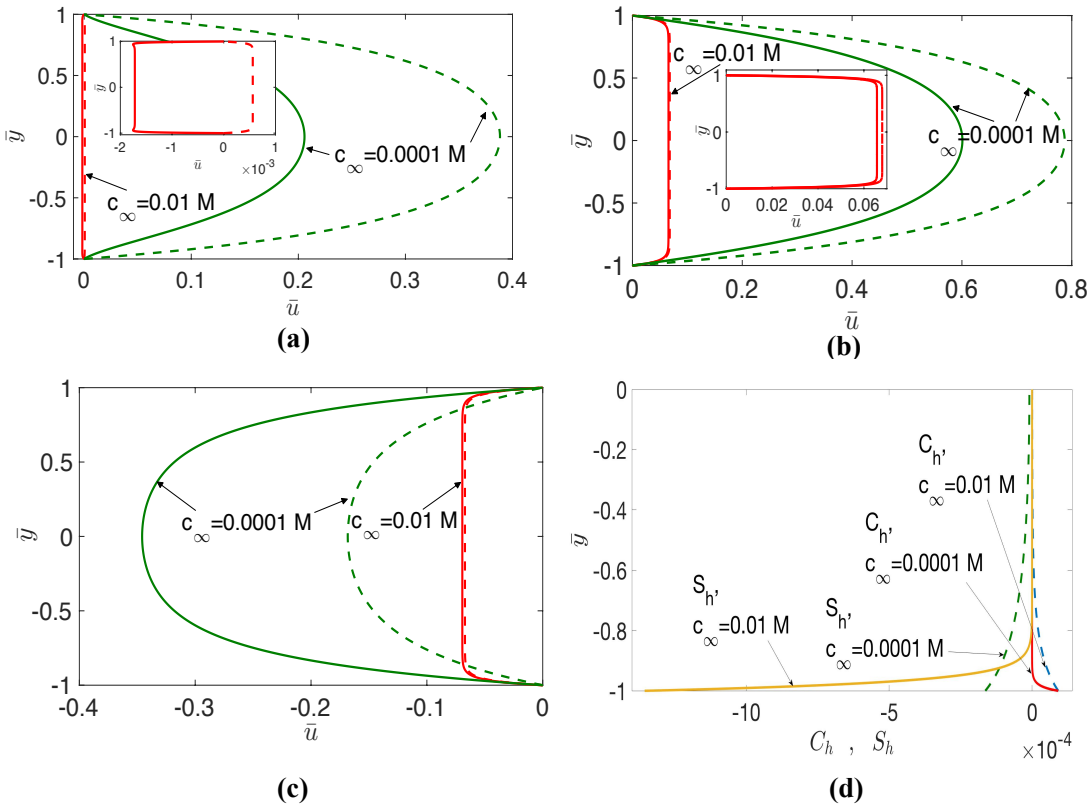

Figure 2.4: Transverse variation of the dimensionless DOS velocity field (shown by bold lines) and EOS velocity field (obtained by switching off the contribution of the pressure gradient in eq. 15 and shown by dashed lines) for (a) $\beta = 0$, (b) $\beta = 0.5$, and (c) $\beta = -0.5$. In the insets of (a) and (b) the EOS and the DOS velocity fields for $c_\infty = 0.01\ M$ are magnified. (d) Transverse variation (for the nanochannel bottom half) of $C_h = c_\infty \left[\cosh\left(\bar{\psi}\right) - 1\right]$ and $S_h = c_\infty \sinh\left(\bar{\psi}\right)$, both of which are independent of β. The results are shown for the brush-free nanochannels and for two different salt concentrations ($c_\infty = 0.0001\ M,\ 0.01\ M$). Other parameters used in this study are same as that in Fig. 3.

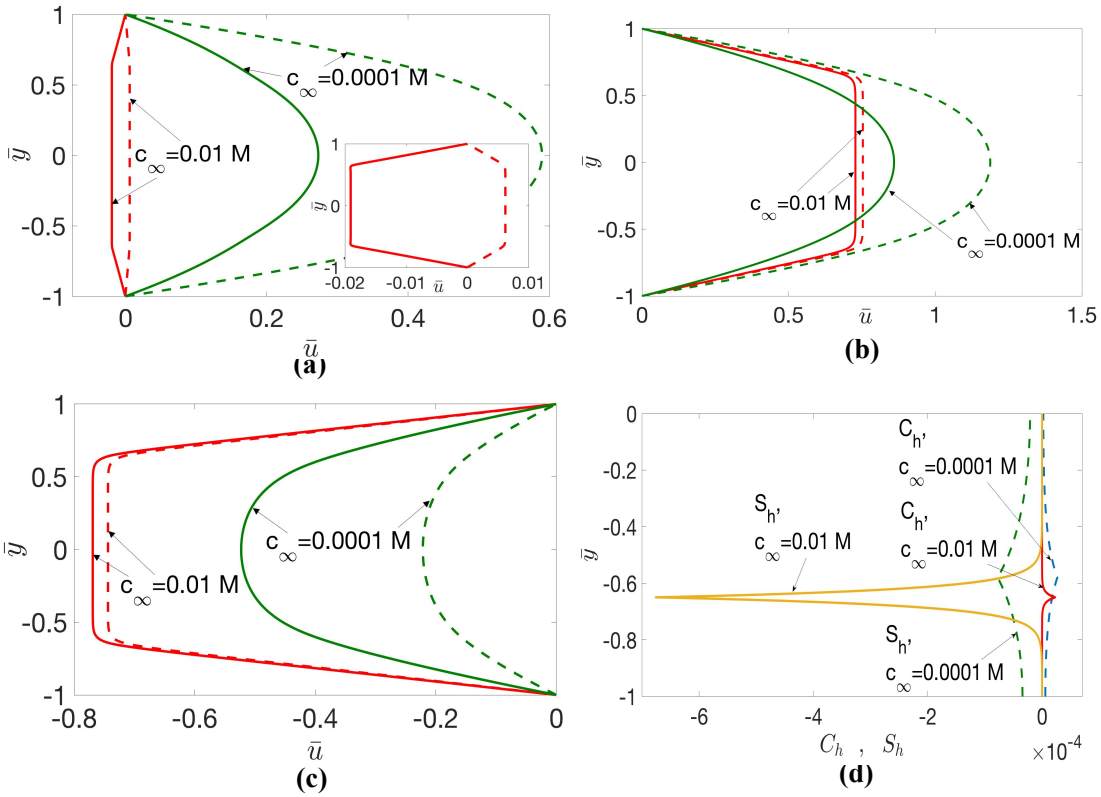

Figure 2.5: Transverse variation of the dimensionless DOS velocity field (shown by bold lines) and EOS velocity field (obtained by switching off the contribution of the pressure gradient in eq. 15 and shown by dashed lines) for (a) $\beta = 0$, (b) $\beta = 0.5$, and (c) $\beta 0.5$. In the inset of (a) the EOS and the DOS velocity fields for $c_\infty = 0.01\ M$ are magnified. (d) Transverse variation (for the nanochannel bottom half) of $C_h = c_\infty \left[\cosh\left(\bar{\psi}\right) - 1\right]$ and $S_h = c_\infty \sinh\left(\bar{\psi}\right)$, both of which are independent of β. The results are shown for the brush-grafted nanochannels (with $N_p = 2000$ and $\ell = 80\ nm$) and for two different salt concentrations ($c_\infty = 0.0001\ M,\ 0.01\ M$). Other parameters used in this study are same as that in Fig. 3.

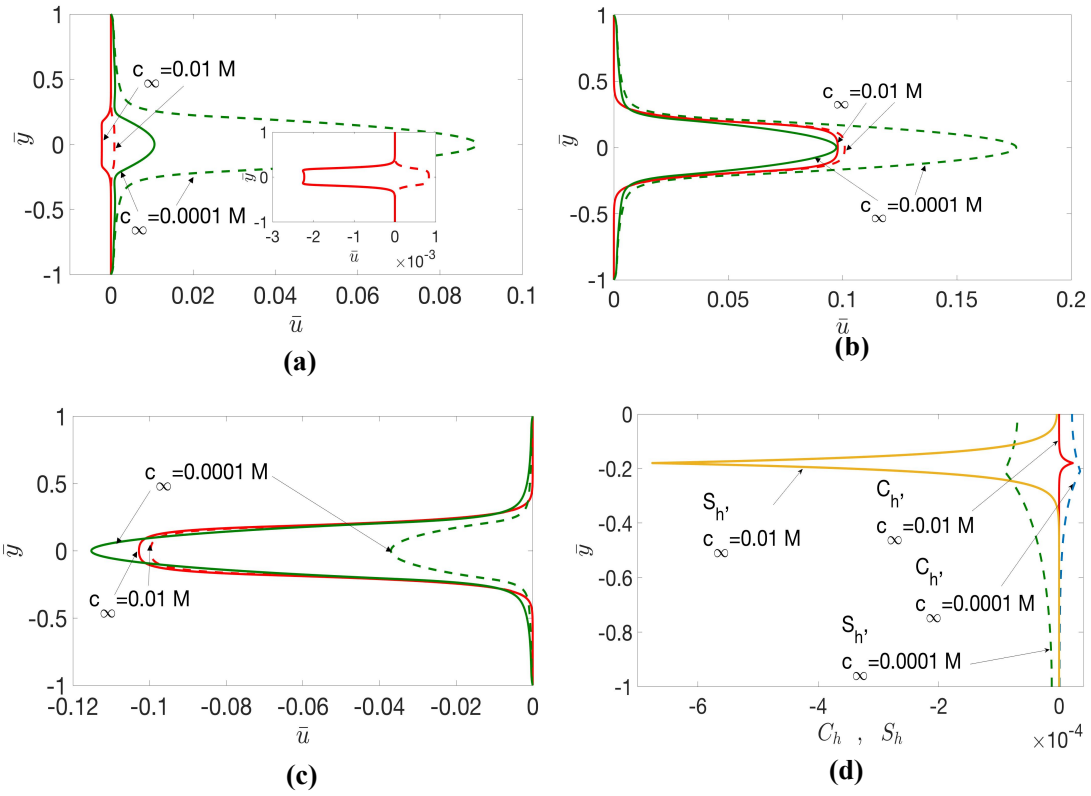

Figure 2.6: Transverse variation of the dimensionless DOS velocity field (shown by bold lines) and EOS velocity field (obtained by switching off the contribution of the pressure gradient in eq. 15 and shown by dashed lines) for (a) $\beta = 0$, (b) $\beta = 0.5$, and (c) $\beta = -0.5$. In the inset of (a) the EOS and the DOS velocity fields for $c_\infty = 0.01\ M$ are magnified. (d) Transverse variation (for the nanochannel bottom half) of $C_h = c_\infty \left[\cosh\left(\bar{\psi}\right) - 1\right]$ and $S_h = c_\infty \sinh\left(\bar{\psi}\right)$, both of which are independent of β. The results are shown for the brush-grafted nanochannels (with $N_p = 2000$ and $\ell = 22\ nm$) and for two different salt concentrations ($c_\infty = 0.0001\ M,\ 0.01\ M$). Other parameters used in this study are same as that in Fig. 3.

COS velocity is triggered on account of the axial pressure gradient induced by the imposition of the axial CG. In order to distinguish between the relative contributions of the EOS and the COS velocity fields in deciding the overall DOS velocity field, in Figs. 4-6 we plot both the overall DOS velocity field as well as only the EOS velocity field (obtained by switching off the pressure gradient term in eq. 15). We first consider the case of brush free nanochannels with $\beta = 0$ [see Fig. 4(a)]. For this condition the induced DOS electric field (E) is positive for all values of c_∞ [see Fig. 3(a)] with E increasing drastically with a decrease in c_∞. Consequently, the EOS velocity field is invariably positive (i.e., occurs from left to right) and increases significantly with a decrease in c_∞. However, the overall DOS velocity field bears the signature of the contribution of the COS component as well. Accordingly, there is a significant reduction in the net velocity (i.e, the DOS velocity) as compared to the pure EOS velocity stemming from the fact that the COS velocity being caused by a positive pressure gradient is invariably negative (i.e., opposes the EOS flow caused by a positive electric field). Dimensionless COS body force, for a given value of imposed $\frac{L\nabla n_\infty}{n_\infty}$, is proportional to $C_h = c_\infty[\cosh(\bar{\psi}) - 1]$, arising from the fact that from eq.(16) we get the dimensionless pressure gradient (or the dimensionless per unit volume COS body force) as $A\bar{n}_1'[\cosh(\bar{\psi}) - 1] = \frac{2k_BT\nabla n_\infty h^2}{\eta U^*}[\cosh(\bar{\psi}) - 1] = \left(\frac{2k_BTh^2}{\eta U^* L}\right)\left(\frac{L\nabla n_\infty}{n_\infty}\right) n_\infty[\cosh(\bar{\psi}) - 1] = 10^3 N_A \left(\frac{2k_BTh^2}{\eta U^* L}\right)\left(\frac{L\nabla n_\infty}{n_\infty}\right) c_\infty[\cosh(\bar{\psi}) - 1]$ (where c_∞ is the concentration in M and N_A is the Avogadro number). Fig. 4(d) provides the transverse variation of C_h, which is independent of β, for two different values of c_∞ for the case of brush free nanochannels. C_h is present only within the EDL and hence non-existent at locations even slightly away from the nanochannel wall for

large salt concentrations. This justifies a much lesser retarding contribution of the COS velocity field for larger c_∞. Hence we witness the overall DOS velocity field to be much smaller than the EOS velocity field for smaller c_∞. However, the EOS velocity field is very small for a larger c_∞ owing to a significantly weaker electric field; accordingly, we witness an actual inversion (i.e., a flow field from right to left) of the entire DOS velocity field on account of the retarding influence of the COS velocity.

We next consider the case of $\beta = 0.5$ for the brush-free nanochannels [see Fig. 4(b)]. For such a positive value of β, the electric field is significantly enhanced [see Fig. 3(a)] causing a significantly larger induced EOS velocity field. Here too an increase in salt concentration lowers this electric field [see Fig. 3(a)] and hence the EOS velocity field and also lowers the retarding COS velocity component (as evident from the lowering of the corresponding COS body force, see Fig. 4(d)] thereby reducing the difference between the overall DOS velocity and the EOS velocity. Of course, for this case the electric field and the EOS velocity is significantly larger and positive even for large c_∞ ensuring a net positive DOS velocity field for such c_∞. It is worthwhile to note here that the EOS body force, in addition to being proportional to the electric field E, is also proportional to $S_h = c_\infty \sinh(\bar{\psi})$ stemming from the fact that the EOS body force varies as $A \sinh(\bar{\psi}) = \frac{2k_B T h^2}{L\eta U^*} n_\infty \sinh(\bar{\psi}) = 10^3 N_A \frac{2k_B T h^2}{L\eta U^*} c_\infty \sinh(\bar{\psi})$ [see eq.(16)]. In Fig. 4(d), we also plot S_h, which being finite only within the EDL will be non-existent at locations slightly away from the nanochannels wall for large c_∞. Therefore, for $\beta = 0, 0.5$, the electroosmotic flow is enhanced for a smaller salt concentration due to a combined action of larger electric field [see Fig. 3(a)] and a larger S_h.

Finally, we consider the case of $\beta = -0.5$ for brush-free nanochannels [see Fig. 4(c)]. Here the electric field is negative [see Fig. 3(a)], and consequently the EOS flow will also be negative, i.e., from right to left. However, as evident from Fig. 3(a), for $\beta = -0.5$, the negative magnitude of the electric field is larger for larger c_∞. Despite that, we witness a larger magnitude of the negative EOS velocity for weaker c_∞, stemming from the fact that the component S_h is significantly larger (particularly at locations slightly away from the wall) for smaller c_∞. Secondly, given the fact that the EOS velocity field is negative, the negative COS velocity will *augment* the net DOS flow rather than decreasing it. Obviously the COS velocity component is larger in magnitude for smaller c_∞, owing to a larger COS body force for smaller c_∞ [see Fig. 4(d)]. Accordingly, one will witness a significantly larger (and significantly augmented as compared to the pure EOS velocity field) DOS velocity field occurring from right to left for such small c_∞ values. In summary, therefore, we establish the manner in which parameters such as β and c_∞ interplay to dictate the relative contribution of the EOS and the COS velocity fields to dictate the overall DOS velocity field in the brush-free nanochannel.

Case of brush-grafted nanochannels ($N_p = 2000,\ \ell = 80\ nm$***):***

For the brush-grafted nanochannels, we first consider the case of long, weakly grafted brushes (quantified by $N_p = 2000$, $\ell = 80\ nm$). We start with the case of $\beta = 0$ [see Fig. 5(a)]. As evident from Fig. 3(b), very much like the case of brush-free nanochannels, the electric field is positive and increases with a decrease in c_∞. Therefore, there

will be a positive EOS flow that increases significantly with a decrease in c_∞. Also, very much like the case of the brush-free nanochannels, the variable C_h dictating the body force for the COS flow (which occurs from right to left) massively increases for smaller c_∞ particularly at locations slightly away from the location of the maximum charge density (i.e., the non-grafted charged end of the brushes) [see Fig. 5(d)]. Therefore, here too the DOS velocity will be significantly weaker than the EOS velocity for smaller c_∞. However, given that the EOS velocity itself is distinctly small for a larger c_∞, the retarding influence of the COS velocity will eventually lead to a reversal in the direction of the overall DOS velocity for large c_∞.

We next consider the case of $\beta = 0.5$ [see Fig. 5(b)]. The significantly large positive electric field [see Fig. 3(b)] will lead to a significantly larger positive EOS velocity that increases with a decrease in c_∞. Of course, here too, the retarding influence of the COS velocity reduces the flow strength and this reduction is much more prominent for weaker c_∞. It is worthwhile to compare the velocity profiles with those of the brush-free nanochannels at this point. Despite the electric field values being similar for both brush-free and brush-grafted nanochannels, we witness (i) a distinctly higher magnitude of both the EOS and the DOS velocities for a given c_∞ [compare Figs. 4(b) and 5(b)] and (ii) there is a much lesser difference between the DOS velocities at different salt concentrations [compare Figs. 4(b) and 5(b)]. We can ascribe both of these effects to the charge localization induced enhancement in the EDL-induced EOS transport [49]. The EDL is invariably localized around the charged ends of the PE brushes. The EOS body force is proportional to the charge density difference within the EDL and therefore would be maximum around these

charged ends of the PE brushes. These charged ends being significantly away from the wall would imply the maximum drag force caused by the wall will be significantly away from the location of the maximum driving body force. This would imply that a same driving EOS body force would lead to a larger EOS velocity. Obviously this enhancement is countered by the additional drag induced by the presence of the brushes. This countering influence is overcome for the case of weak brush grafting density and significantly large N_p (e.g., the present case of $N_p = 2000$ and $\ell = 80\ nm$), leading to the most non-intuitive scenario where the EOS flow strength is actually enhanced by the presence of the brushes [49]. This justifies why one witnesses a much larger EOS velocity (and hence a larger DOS velocity) for nearly similar electric field (or similar combinations of β and c_∞) for the brush-grafted nanochannels (with $N_p = 2000$ and $\ell = 80\ nm$) as compared to the brush-free nanochannels. Of course, in Chen and Das [49], the EOS flow was triggered by an applied electric field, while in the present case, it is induced due to diffusioosmosis. Secondly, this localization of the EDL around the charged end of the end-charged PE brushes is more prominent for larger salt concentration (which causes a smaller EDL). Accordingly, this EDL localization induced localization of the driving EOS body force is more prominent for larger c_∞, leading to a larger enhancement of the EOS (and hence DOS) velocity fields for larger c_∞. This justifies the second observation that for brush-grafted nanochannels the difference in the EOS (and hence DOS velocity fields) between large and small salt concentration values are much less, despite the electric field being much larger for smaller salt concentration (for $\beta = 0, 0.5$).

Finally, we consider the case of $\beta = -0.5$ [see Fig. 5(c)]. Here the electric field

is negative [see Fig. 3(b)] and the magnitude of the electric field increases with an increase in salt concentration. Coupled with this effect is the fact that the effect of EDL localization and the resulting enhancement in the EOS transport [49] is much more enhanced for the case of larger c_∞. These two effects overcome the effect of a reduced S_h for larger concentration, eventually ensuring a much larger negative magnitude of the EOS transport for larger c_∞. Of course, as with the case of brush-free nanochannels here the COS velocity, which is itself negative, will augment the EOS flow strength leading to a DOS flow that is more enhanced than the EOS flow. Comparing with the case of the brush-free nanocahnnels [see Fig. 4(c)], here we witness that the EOS body force localization effect associated with the EOS transport in nanochannels grafted with end-charged brushes not only enhnaces the magnitude of the EOS (and hence DOS) velocity fields, but also causes a reversal in the salt-concentration-dependence of the velocity field.

Case of brush-grafted nanochannels ($N_p = 2000,\ \ell = 22\ nm$)***:***

We finally consider the case of brush-grafted nanochannels with large grafting density ($\ell = 22\ nm$). A large grafting density will impart such a large drag force on the flow that the effect of EDL (and hence the EOS body force) localization will be nullified leading to a decrease in the overall velocity field. Obviously the decrease is most stark at transverse locations deep within the brushes depicting a virtually non-existent velocity. Also, very much like the case of brush-free nanochannels and naochannels grafted with less dense brushes, we witness a negative DOS velocity for

large c_∞ and $\beta = 0$. On the other hand, the EDL charge density and EOS body force localization effect ensures very little difference in the EOS (and hence DOS) velocities between the cases of large and small salt concentrations for $\beta = 0.5$. Finally for $\beta = -0.5$, the negative electric field causes a negative EOS velocity field, which is much larger for larger c_∞ owing to the combined influence of enhanced magnitude of the negative electric field [see Fig. 3(c)] and the flow enhancement due to a stronger localization of the EOS body force away from the nanochannel walls. On the other hand, the significantly larger value of C_h [and hence the COS velocity, see Fig. 6(d)] for a smaller c_∞ outweighs this enhanced EOS velocity and eventually ensures that the magnitude of the overall DOS velocity is very much similar.

2.4 Conclusions

We develop theory to study the problem of IDO in end-charged brush-grafted nanochannels. We show that the weird fluid physics of augmented EOS transport in such systems, owing to the localization of the EDL charge density and the EOS body force away from the nanochannel wall, can be successfully leveraged to develop an extremely augmented DOS fluid transport in nanochannels grafted with long and weakly dense brushes. This augmentation is with respect to brush-free nanochannels and depend on the exact extent of the influence of the COS transport. Depending on the relative magnitude of the counterion and coion diffusivities, this COS transport may augment or retard the EOS tranpsort in deciding the overall DOS transport. The effect of end-charge localization in augmenting the flow is found to be the most

prominent for the case where the COS transport aids the EOS transport. We anticipate that this paper will bring to light a new mechanism of electrokinetic transport in functionalized nanochannels that can be successfully used for a myriad of flow-field-dependent and hitherto unconceived applications in such nanochannels.

Appendix

Derivation of eq. 2.13

Eq.(13) expresses the diffusioosmotically induced electric field obtained by making the net current equal to zero, i.e., $\int_{-h}^{h}(J_+ - J_-)\,dy = 0$. The flux $J_\pm$ can be expressed as (considering $n_\pm = n_\infty e^{\mp\bar{\psi}}$ so that $\nabla n_\pm = \nabla n_\infty e^{\mp\bar{\psi}} \mp n_\infty e^{\mp\bar{\psi}}\nabla\bar{\psi}$):

$$\begin{aligned}
J_\pm = &-D_\pm\left[\nabla n_\pm \pm \frac{e}{k_BT}n_\pm\left(\nabla\psi - E\right)\right] + n_\pm u = \\
&- D_\pm\left[\nabla n_\infty e^{\mp\bar{\psi}} \mp \left(n_\infty e^{\mp\bar{\psi}}\right)\nabla\bar{\psi} \pm \frac{e}{k_BT}n_\pm\left(\nabla\psi - E\right)\right] + n_\pm u = \\
&- D_\pm\left[\nabla n_\infty e^{\mp\bar{\psi}} \mp \frac{e}{k_BT}n_\pm\nabla\psi \pm \frac{e}{k_BT}n_\pm\left(\nabla\psi - E\right)\right] + n_\pm u = \\
&\quad D_\pm\left[\nabla n_\infty e^{\mp\bar{\psi}} \mp \frac{e}{k_BT}n_\pm E\right] + n_\pm u
\end{aligned} \tag{A1}$$

We can calculate the electric field by equating the net current to zero, i.e.,

$$\begin{aligned}
&\int_{-h}^{h}(J_+ - J_-)\,dy = 0 \Rightarrow \\
&-D_+\int_{-h}^{h}\left[\nabla n_\infty e^{-\bar{\psi}} - \frac{e}{k_BT}n_+E\right]dy + \int_{-h}^{h}n_+u dy = -D_-\int_{-h}^{h}\left[\nabla n_\infty e^{\bar{\psi}} + \frac{e}{k_BT}n_-E\right]dy \\
&\qquad\qquad + \int_{-h}^{h}n_-u dy \Rightarrow \\
&\frac{e}{k_BT}E\int_{-h}^{h}\left(D_+n_+ + D_-n_-\right)dy = \int_{-h}^{h}u\left(n_- - n_+\right)dy + \int_{-h}^{h}\left(D_+\nabla n_\infty e^{-\bar{\psi}} - D_-\nabla n_\infty e^{\bar{\psi}}\right)dy
\end{aligned} \tag{A2}$$

Also, considering $\beta = \frac{D_+ - D_-}{D_+ + D_-}$, we can write:

$$D_+ = \frac{(1+\beta)(D_+ + D_-)}{2},\ D_- = \frac{(1-\beta)(D_+ + D_-)}{2}. \tag{A3}$$

Using eqs.(A3), we can write:

$$D_+ n_+ + D_- n_- = \frac{D_+ + D_-}{2} n_\infty \left[(1+\beta)\, e^{-\bar{\psi}} + (1-\beta)\, e^{\bar{\psi}}\right]. \tag{A4}$$

$$D_+ \nabla n_\infty e^{-\bar{\psi}} - D_- \nabla n_\infty e^{\bar{\psi}} = \frac{D_+ + D_-}{2} \frac{\bar{n}_1' n_\infty}{L} \left[(1+\beta)\, e^{-\bar{\psi}} - (1-\beta)\, e^{\bar{\psi}}\right], \tag{A5}$$

where

$$\bar{n}_1' = \frac{L \nabla n_\infty}{n_\infty}. \tag{A6}$$

Finally we can write:

$$u\,(n_- - n_+) = 2 n_\infty u \sinh(\bar{\psi}). \tag{A7}$$

Using eqs.(A4,A5,A7), we can finally obtain from eq.(A2) as:

$$E = \frac{k_B T}{e} \frac{\int_{-h}^{h} 4u \sinh(\bar{\psi}) dy}{(D_+ + D_-) \int_{-h}^{h} \left[(1+\beta)\, e^{-\bar{\psi}} + (1-\beta)\, e^{\bar{\psi}}\right] dy} +$$
$$\frac{k_B T}{eL} \frac{\int_{-h}^{h} \bar{n}_1' \left[(1+\beta_1)\, e^{-\bar{\psi}} - (1-\beta_1)\, e^{\bar{\psi}}\right] dy}{\int_{-h}^{h} \left[(1+\beta)\, e^{-\bar{\psi}} + (1-\beta)\, e^{\bar{\psi}}\right] dy} \Rightarrow$$
$$\bar{E} = \frac{E}{E_0} = Pe \frac{\int_{-1}^{1} 4\bar{u} \sinh(\bar{\psi}) dy}{\int_{-1}^{1} \left[(1+\beta)\, e^{-\bar{\psi}} + (1-\beta)\, e^{\bar{\psi}}\right] d\bar{y}} + \frac{\int_{-1}^{1} \bar{n}_1' \left[(1+\beta)\, e^{-\bar{\psi}} - (1-\beta)\, e^{\bar{\psi}}\right] d\bar{y}}{\int_{-1}^{1} \left[(1+\beta)\, e^{-\bar{\psi}} + (1-\beta)\, e^{\bar{\psi}}\right] d\bar{y}},$$

where $E_0 = \frac{k_B T}{eL}$, $\bar{u} = \frac{u}{U^*}$, $Pe = U^* L / (D_+ + D_-)$.

Derivation of eq. 2.16

For the bottom half of the nanochannel, the Navier Stokes equation for the x-momentum for the location within the PE brushes can be expressed as [using eq.(14)

to express p so that $\frac{\partial p}{\partial x} = 2k_BT\nabla n_\infty\left[\cosh\left(\bar{\psi}\right)-1\right] + 2k_BTn_\infty\left[\sinh\left(\bar{\psi}\right)\nabla\bar{\psi}\right]$]:

$$\eta\frac{d^2u}{dy^2} = \frac{\partial p}{\partial x} + \eta\frac{u}{k_d} - e\left(n_+ - n_-\right)\left(E - \nabla\psi\right) \qquad for\ -h \le y \le -h+d \Rightarrow$$

$$\eta\frac{d^2u}{dy^2} = 2k_BT\nabla n_\infty\left[\cosh\left(\bar{\psi}\right)-1\right] + 2k_BTn_\infty\left[\sinh\left(\bar{\psi}\right)\nabla\bar{\psi}\right] +$$

$$\eta\frac{u}{k_d} + 2en_\infty\sinh\left(\bar{\psi}\right)E - 2k_BTn_\infty\left[\sinh\left(\bar{\psi}\right)\nabla\bar{\psi}\right]$$

$$\frac{\eta U^*}{h^2}\frac{d^2\bar{u}}{d\bar{y}^2} = 2k_BT\frac{n_\infty}{L}\left\{\left(\frac{L\nabla n_\infty}{n_\infty}\right)\left[\cosh\left(\bar{\psi}\right)-1\right]\right\} + \frac{\eta U^*}{k_d}\bar{u} + 2eE_0L\frac{n_\infty}{L}\sinh\left(\bar{\psi}\right)\bar{E}$$

$$for\ -1 \le \bar{y} \le -1+\bar{d} \Rightarrow$$

$$\frac{d^2\bar{u}}{d\bar{y}^2} = A\left\{\bar{n}_1'\left[\cosh\left(\bar{\psi}\right)-1\right]\right\} + \alpha^2\bar{u} +$$

$$A\sinh\left(\bar{\psi}\right)\left\{Pe\frac{\int_{-1}^{1}4\bar{u}\sinh\left(\bar{\psi}\right)dy}{\int_{-1}^{1}\left[\left(1+\beta\right)e^{-\bar{\psi}} + \left(1-\beta\right)e^{\bar{\psi}}\right]d\bar{y}} + \frac{\int_{-1}^{1}\bar{n}_1'\left[\left(1+\beta\right)e^{-\bar{\psi}} - \left(1-\beta\right)e^{\bar{\psi}}\right]d\bar{y}}{\int_{-1}^{1}\left[\left(1+\beta\right)e^{-\bar{\psi}} + \left(1-\beta\right)e^{\bar{\psi}}\right]d\bar{y}}\right\}$$

$$for\ -1 \le \bar{y} \le -1+\bar{d}.$$

Of course, by the same procedure as employed above, we can show:

$$\eta\frac{d^2u}{dy^2} = \frac{\partial p}{\partial x} + \eta\frac{u}{k_d} - e\left(n_+ - n_-\right)\left(E - \nabla\psi\right) \qquad for\ -h+d \le y \le 0 \Rightarrow$$

$$\frac{d^2\bar{u}}{d\bar{y}^2} = A\left\{\bar{n}_1'\left[\cosh\left(\bar{\psi}\right)-1\right]\right\} +$$

$$A\sinh\left(\bar{\psi}\right)\left\{Pe\frac{\int_{-1}^{1}4\bar{u}\sinh\left(\bar{\psi}\right)dy}{\int_{-1}^{1}\left[\left(1+\beta\right)e^{-\bar{\psi}} + \left(1-\beta\right)e^{\bar{\psi}}\right]d\bar{y}} + \frac{\int_{-1}^{1}\bar{n}_1'\left[\left(1+\beta\right)e^{-\bar{\psi}} - \left(1-\beta\right)e^{\bar{\psi}}\right]d\bar{y}}{\int_{-1}^{1}\left[\left(1+\beta\right)e^{-\bar{\psi}} + \left(1-\beta\right)e^{\bar{\psi}}\right]d\bar{y}}\right\}$$

$$for\ -1+\bar{d} \le \bar{y} \le 0.$$

(B1)

Chapter 3: Seebeck Effect and Ionic Thermo-osmosis in Nanochannels Grafted with End-charged Polyelectrolyte Brushes

In this chapter[1]*, we develop a theory to study the imposed axial temperature-gradient-driven Seebeck effect and ionic thermoosmosis (ITO) in soft nanochannels or nanochannels grafted with end-charged polyelectrolyte (PE) brushes. Our analysis first quantifies the thermoosmotically induced electric field. This electric field results from three effects: (a) advective separation of the EDL charge density, (b) Soret effect due to the imposed temperature gradient caused by the differences in the thermophoretic mobility of the ions, and (c) the EDL induced electrophoretic effect modified by the diffusivity differences of the cations and counterions. This induced electric field triggers an electroosmostic (EOS) transport, while the net thermoosmotic (TOS) transport results from a combination of this EOS transport and a combined thermo-chemioosmotic (TCOS) transport arising from the pressure gradient induced by the applied temperature gradient and the induced (in a direction opposite to the temperature gradient)*

[1]Contents of this chapter have been submitted as *R. S. Maheedhara, H. Jing, and S. Das, "Highly enhanced liquid flows via thermoosmotic effects in soft and charged nanochannels," Phys. Chem. Chem. Phys (submitted)*

concentration gradient. Our results unravel that the TOS transport is massively enhanced in nanochannels grafted with PE brushes with weak grafting density stemming from the significantly enhanced EOS transport caused by the localization of the EOS body force away from the nanochannel walls. This augmentation is even stronger for cases where the TCOS transport aids the EOS transport. On the other hand, the TOS transport gets severely reduced in nanochannels grafted with dense PE brushes owing to the severity of the brush-induced additional drag force. We anticipate that these findings will help to unravel an entirely new understanding of induced electrokinetic transport in soft nanochannels.

3.1 Introduction

Seebeck effect refers to the generation of an electric field in presence of a temperature gradient [96, 97]. While Seebeck effect has been considered for different materials and under different conditions [96–100], here we only focus on the Seebeck effect in an ionic system (e.g., an electrolyte solution) in presence of an external axially imposed temperature gradient [101–106]. Classically, one obtains the Seebeck coefficient quantifying the Seebeck effect, when this electric field is divided by this temperature gradient. For a simple electrolyte system that is charge neutral at every location and the ions are assumed to havese identical mobilities, this electric field (and hence the Seebeck effect) is simply proportional to the axial temperature gradient and the difference in the thermophoretic mobilities of the ions [106]. This electric field can be considered as the Soret electric field as it depends on the thermophoretic mobility

of the ions. Dietzel and Hardt [107] studied the same problem for the case where the temperature gradient is employed across the charged nanochannel, i.e., where there is a significant influence of the EDL. For such a case, this idea of charge neutrality no longer holds within the EDL. As a consequence, this Soret electric field gets altered and contains the contribution of the EDL electrostatic potential. In addition, the presence of the EDL leads to another component of the electric field that depends on the electrophoretic mobilities of the ions and can be termed as the Electrophoretic electric field. Of course, Dietzel and Hardt considered identical diffusivities of the ions. In a separate study, Dietzel and Hardt [108] did consider the thermoosmotic flow field and provided a detailed mathematics to analyze the flow field in presence of the unequal ionic mobilities. It is worthwhile to mention here that there have been other studies that have attempted to exploit the EDL effects in a nanoconfinement for the generation of Seebeck effect [109, 110]; however, the studies by Dietzel and Hardt [107,108] can be considered to be the state of the art in theoretical understanding of the problem of EDL regulated Seebeck effect and thermoosmotic transport in charged nanochannels.

In our study, we probe the TOS flow and Seebeck effect in a soft, charged nanochannel (i.e., a nanochannel grafted with end-charged PE brushes). For that purpose we consider a reformulation of Ref. [107] by considering different diffusivities of the ions as well as a finite contribution of the advective flux. Of course, Ref. [107] includes these issues; however, we solve a simplistic system similar to Ref. [107] where the EDL electrostatics and the ion distribution are decoupled from the flow field (i.e., not governed by the Nernst-Planck equation). Under this condition, there is a com-

ponent of the electric field in addition to the Soret electric field and Electrophoretic electric field: this component is the Advective electric field caused by the advective transport of the ion imbalance within the EDL. Of course, the consideration of different diffusivities of the ions would imply alteration in even the Soret electric field and Electrophoretic electric field. Secondly, this velocity field u, which is used to quantify the advective electric field, is not known apriori. Rather it has to be calculated using the steady-state Stokes equation (Navier Stokes equation without the non-linear advection terms). The velocity field is a combination of two effects. Firstly, this induced electric field (consisting of the three different contributions) drives an electroosmtic (EOS) transport. Secondly, the presence of an axial temperature gradient and an axial gradient in the bulk ion concentration (attributed to the axial temperature gradient) leads to an axial pressure gradient, which drives a flow. This flow component, therefore, can be termed as thermo-chemoosmotic (TCOS) transport. Hence the flow field is a combination of the EOS and the TCOS transport. Obviously, this EOS transport being dependent on the velocity field itself, we would effectively need to first solve an integro-differential equation to obtain u. After that, this information of u can be used to quantify the overall electric field. Given this elaborative framework for probing the Seebeck effect and the TOS transport in charged nanochannels, we focus on the calculations for a soft and charged nanochannel. The softness of the nanochannel is attributed to the presence of end-charged brushes grafted on the inner walls of the nanochannel. The presence of these brushes change the EDL electrostatic potential distribution as well as imparts an additional drag force on the fluid flow. These effects are appropriately accounted for in our model. The key significance is

that under certain conditions of grafting and brush parameters, we can witness the most remarkable situation where this EDL re-organization (or localization) induced EOS body force can be so influential (since it is localized significantly away from the location of the maximum drag, i.e., the nanochannel walls) that it can overcome the effect of the additional drag imposed by the presence of the brushes. The result is a TOS transport that is significantly augmented in brush-grafted nanochannels as compared to the brush-free nanochannels.

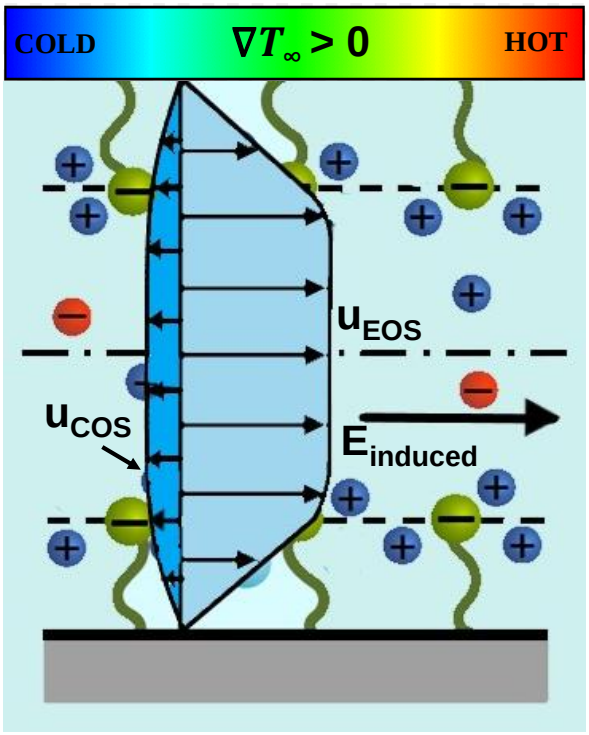

Figure 3.1: Schematic showing the TOS transport in nanochannels grafted with end-charged brushes. The TOS flow is a combination of the EOS (caused by the induced electric field) and the TCOS flows, as illustrated in the schematic.

3.2 Theory

We consider a nanochannel of half height h and length L grafted with end-charged PE brushes (see Fig. 3.1). The nanochannel is connected to bulk microfluidic reservoirs. We have previously studied the electrostatics, thermodynamics, ionic current, and electrokinetic transport in such nanochannels. The calculation of the electrokinetic transport in these papers is unique in the sense that it accounts for the appropriate coupling of the brush configuration and the resulting EDL electrostatics while computing the electrokinetic fluid flow. In the present paper, we would use this

information on the coupled brush configuration and the resulting EDL electrostatics in order to quantify the ionic TOS transport. The TOS transport is triggered by imposing a constant axial temperature gradient of strength $\nabla T = dT_\infty/dx$, such that $L\nabla n_\infty/n_\infty(x=0) \ll 1$ (here $\frac{\nabla n_\infty}{n_\infty}$ is the concentration gradient induced because of the applied temperature gradient; n_∞ is the bulk number density of the electrolyte ions or the electrolyte ion concentration in the microfluidic reservoirs) as well as $L\nabla T_\infty/T_\infty(x=0) \ll 1$. The coupled equilibrium description of the configuration of the end-charged PE brush and the induced EDL electrostatics has already been provided in our previous paper [49] – we shall use this equilibrium description to quantify the electric field induced due to the thermoosmotic effect and the resulting nanofluidic velocity field (occurring due to the combined influence of the induced EOS and the TCOS velocities).

3.2.1 Thermoosmotically Induced Electric Field

In order to obtain the thermoosmotically induced electric field, we need to equate the net current in the system to zero, which is identical to making the integral of the difference between the cationic and anionic fluxes to zero, i.e.,

$$\int_{-h}^{h} (J_+ - J_-)\, dy = 0, \tag{3.1}$$

where the fluxes ($J_\pm$) can be expressed as:

$$J_\pm = -D_\pm \left[\nabla n_\pm \pm \frac{e}{k_B T} n_\pm (\nabla\psi - E) + \frac{Q_\pm}{k_B T^2} n_\pm \nabla T\right] + n_\pm u. \tag{3.2}$$

In the above equation, $D_\pm$ are the diffusivities of cations and anions, u is the induced velocity field (a combination of the EOS and TCOS velocity fields), $Q_\pm$ are the heats

of transport of cations and anions, and E is the induced electric field. Using eq.(3.2) in eq.(3.1), we shall eventually get the dimensionless thermoosmotically induced electric field (please see the Appendix for detailed derivation):

$$\bar{E} = \frac{E}{E_0} = \frac{\nabla T}{T}\left\{\frac{-\Pi\left\{\int_{-1}^{1} Pe\sinh\left(\bar{\psi}\right)\bar{u}d\bar{y} + \int_{-1}^{1}\left[\left(1+\beta\right)e^{-\bar{\psi}} - \left(1-\beta\right)e^{\bar{\psi}}\right]d\bar{y}\right\}}{\int_{-1}^{1}\left[\left(1+\beta\right)e^{-\bar{\psi}} + \left(1-\beta\right)e^{\bar{\psi}}\right]d\bar{y}}\right\} + \frac{\nabla T}{T}\left\{\frac{\Gamma\int_{-1}^{1}\left[\left(1+\alpha\right)e^{-\bar{\psi}} - \left(1-\alpha\right)e^{\bar{\psi}}\right]d\bar{y}}{\int_{-1}^{1}\left[\left(1+\beta\right)e^{-\bar{\psi}} + \left(1-\beta\right)e^{\bar{\psi}}\right]d\bar{y}}\right\}, \tag{3.3}$$

where $\bar{y} = y/h$, $E_0 = k_BT/(eL)$, $\bar{u} = u/U^*$ (where U^* is the characteristic velocity scale that defines the Peclet number: $Pe = U^*L/(D_+ + D_-)$), $\bar{\psi} = e\psi/(k_BT)$, $\beta = \frac{D_+ - D_-}{D_+ + D_-}$, $\alpha = \frac{Q_+D_+ - Q_-D_-}{Q_+D_+ + Q_-D_-}$, $\Pi = \frac{Q_+ + Q_-}{2k_BT}$ and $\Gamma = \frac{1}{k_BT}\frac{Q_+D_+ + Q_-D_-}{D_+ + D_-}$.

Finally, the Seebeck Coefficient, S is given by

$$S = \frac{\bar{E}}{\left(\frac{\nabla T}{T}\right)}. \tag{3.4}$$

3.2.2 Thermoosmotic (TOS) Velocity Field

In order to obtain the TOS velocity field, we shall employ the Navier-Stokes (NS) equation. The NS equation in y-direction yields the necessary pressure field, i.e.,

$$\frac{\partial p}{\partial y} + 2e\left(n_+ - n_-\right)\frac{d\psi}{dy} = 0 \Rightarrow p = p_{atm} + 2k_BTn_\infty\left[\cosh\left(\bar{\psi}\right) - 1\right]. \tag{3.5}$$

Finally, the NS equation in the x-direction yields (considering only the nanochannel bottom half):

$$\eta\frac{d^2u}{dy^2} = \frac{\partial p}{\partial x} + \eta\frac{u}{k_d} - e\left(n_+ - n_-\right)\left(E - \nabla\psi\right) \quad for \;\; -h \le y \le -h+d,$$
$$\eta\frac{d^2u}{dy^2} = \frac{\partial p}{\partial x} - e\left(n_+ - n_-\right)\left(E - \nabla\psi\right) \quad for \;\; -h+d \le y \le 0. \tag{3.6}$$

Eq.(3.6) can be expressed in dimensionless form as (see the Appendix for the detailed derivation):

$$\frac{d^2\bar{u}}{d\bar{y}^2} = \left(\bar{\kappa}^2 - \frac{1}{\Pi}\right)\left[\cosh\bar{\psi} - 1\right] + \alpha_0^2\bar{u} -$$
$$\bar{\kappa}^2\sinh\bar{\psi}\left\{\frac{\int_{-1}^{1} Pe\sinh\bar{\psi}\bar{u}d\bar{y} + \int_{-1}^{1}\left[\left(1+\beta\right)e^{-\bar{\psi}} - \left(1-\beta\right)e^{\bar{\psi}}\right]d\bar{y}}{\int_{-1}^{1}\left[\left(1+\beta\right)e^{-\bar{\psi}} + \left(1-\beta\right)e^{\bar{\psi}}\right]d\bar{y}}\right\} -$$
$$\bar{\kappa}^2\sinh\bar{\psi}\left\{\frac{\frac{\Gamma}{\Pi}\int_{-1}^{1}\left[\left(1+\alpha\right)e^{-\bar{\psi}} - \left(1-\alpha\right)e^{\bar{\psi}}\right]d\bar{y}}{\int_{-1}^{1}\left[\left(1+\beta\right)e^{-\bar{\psi}} + \left(1-\beta\right)e^{\bar{\psi}}\right]d\bar{y}}\right\} \qquad for \;\; -1 \le \bar{y} \le -1+\bar{d},$$

$$\frac{d^2\bar{u}}{d\bar{y}^2} = \left(\bar{\kappa}^2 - \frac{1}{\Pi}\right)\left[\cosh\bar{\psi} - 1\right] -$$
$$\bar{\kappa}^2\sinh\bar{\psi}\left\{\frac{\int_{-1}^{1} Pe\sinh\bar{\psi}\bar{u}d\bar{y} + \int_{-1}^{1}\left[\left(1+\beta\right)e^{-\bar{\psi}} - \left(1-\beta\right)e^{\bar{\psi}}\right]d\bar{y}}{\int_{-1}^{1}\left[\left(1+\beta\right)e^{-\bar{\psi}} + \left(1-\beta\right)e^{\bar{\psi}}\right]d\bar{y}}\right\} -$$
$$\bar{\kappa}^2\sinh\bar{\psi}\left\{\frac{\frac{\Gamma}{\Pi}\int_{-1}^{1}\left[\left(1+\alpha\right)e^{-\bar{\psi}} - \left(1-\alpha\right)e^{\bar{\psi}}\right]d\bar{y}}{\int_{-1}^{1}\left[\left(1+\beta\right)e^{-\bar{\psi}} + \left(1-\beta\right)e^{\bar{\psi}}\right]d\bar{y}}\right\} \qquad for \;\; -1+\bar{d} \le \bar{y} \le 0, \tag{3.7}$$

where $\bar{d} = d/h$, η is the dynamic viscosity, and $\alpha_0 = h^2/k_d$ [where $k_d = a_k^2\left(\frac{d}{\sigma a_k^3 N_p \phi}\right)^2$ is the permeability, with ϕ being the monomer distribution along the length of the PE brush]. It is obvious that we arrive at eq.(3.7) by using the expression of E [see eq.(A7)]. Eq.(3.7) is an integro-differential equation in $\bar{u}$, which is solved numerically

in presence of the boundary conditions expressed below.

$$(\bar{u})_{\bar{y}=-1} = 0, \quad (\bar{u})_{\bar{y}=(-1+\bar{d})^+} = (\bar{u})_{\bar{y}=(-1+\bar{d})^-},$$
$$\left(\frac{d\bar{u}}{d\bar{y}}\right)_{\bar{y}=(-1+\bar{d})^+} = \left(\frac{d\bar{u}}{d\bar{y}}\right)_{\bar{y}=(-1+\bar{d})^-}, \quad \left(\frac{d\bar{u}}{d\bar{y}}\right)_{\bar{y}=0} = 0. \tag{3.8}$$

Subsequently, this $\bar{u}$ is used to obtain the dimensionless electric field $\bar{E}$ [see eq.(A7)]. Obviously, both the solution for $\bar{u}$ and $\bar{E}$ will depend on $\bar{\psi}$ – section IIA provides a method to calculate $\bar{\psi}$.

3.3 Results and Discussion

3.3.1 Variation of the EDL electrostatic field $\bar{\psi}$

The EDL electrostatic field is dependent only on the charge density of the brushes/walls, and thus this remains unchanged from Fig 2.2. in chapter 2.

3.3.2 Variation of the thermo-osmotically induced electric field and the resulting Seebeck coefficient

Figure 3.2 shows the variation of the Seebeck coefficient (which is proportional to the electric field, see eq. 3.4) with respect to α, β and c_∞ for the nanochannels with and without the brushes. Any effect that creates an axial separation between the counterions and coions will contribute to the electric field. In this light, there are three effects that contribute to the electric field: (a) the advective migration of the unbalanced charges (or the net charge density) within the EDL, (b) the Soret effect caused by the difference in the thermoophoretic mobilities of the coions and the

counterions (the presence of the unequal number of coions and counterions within the EDL as well as the difference in the diffusivities contribute to this component of the electric field) and (c) the gradient in the number density (in a direction opposite to the temperature gradient) caused by the temperature gradient (this component of the electric field only manifests when there is a difference in the diffusivities of the ions and/or the presence of the EDL leads to an imbalance in the number of coions and counterions). As with the DOS transport, the advective migration of the EDL charge density gradient has less influence on the overall electric field (or Seebeck coefficient); as a consequence there is insignificant difference between the cases of nanochannels with and without the PE brushes for a given c_∞, α, and β.

On the other hand, E (or the Seebeck coefficient) varies significantly with c_∞, α, and β. Positive α implies a positive value of the diffusivity modified thermophoretic mobilities, which for the present case of negatively charged wall or brushes, would signify a larger effective thermophoretic mobility of the counterions. As a result, the imposed temperature gradient would lead to a more enhanced axial separation between the counterions and coions leading to a larger positive (or less negative) magnitude of the electric field for a given c_∞ and β. It is for the same reason that a negative α would signify a larger negative (or less positive) magnitude of the electric field for a given c_∞ and β. This is very much evident if we compare the figures for the variation of the Seebeck coefficient (or the electric field) for different α values (see Fig. 3.2).

We next compare the effect of variation of β, which refers to the contribution of the difference in the diffusivities of the coions and counterions and is modified due to

the development of the EDL. The presence of the positive axial temperature gradient (i.e., $\nabla T = dT_\infty/dx > 0$) would induce a negative axial concentration gradient (i.e., $\nabla n_\infty = dn_\infty/dx < 0$). As a consequence $\beta > 0$, which signifies a larger counterion mobility, would imply that the counterions and coions separate axially in a direction opposite to which the positive temperature gradient separates the coions and counterions. As a result, $\beta > 0$ would have the same influence as $\alpha < 0$, while $\beta < 0$ would have the same effect as $\alpha > 0$. Hence for $\beta < 0$, we always witness a larger positive (or less negative) magnitude of the electric field for a given c_∞ and α, while for $\beta < 0$ we encounter a larger negative (or less positive) magnitude of the electric field for a given c_∞ and α.

We finally analyze the effect of the concentration c_∞ (please note that c_∞ and n_∞ are related as $n_\infty = 10^3 N_A c_\infty$, where n_∞ has the units of $1/m^3$, c_∞ has the units of M, and N_A is the Avogadro number). Weaker c_∞ leads to a larger magnitude of the electrostatic potential (see Fig. 2.2) and hence a larger difference between the coions and counterions. Therefore, the cases of positive electric field (caused by such a separation of counterions and coions where the counterions are in excess at the location of a larger T, e.g., for $\alpha > 0$ and $\beta < 0$) are enhnaced for smaller c_∞. On the other hand, the cases of negative electric field (caused by such a separation of counterions and coions where the counterions are in excess at the location of a smaller T, e.g., for $\alpha < 0$ and $\beta > 0$) are enhanced (in magnitude) for larger c_∞. This latter effect signifies a situation where the electric field magnitude is enhanced when the difference between the counterion and coion concentrations is nullified, and such a situation occurs for a larger c_∞ (see Fig. 2.2).

3.3.3 Variation of the TOS velocity field

The TOS velocity field is a combination of the induced electric field (described above) EOS velocity field and the TCOS velocity field resulting from the induced axial pressure gradient. This induced pressure gradient is always positive, as indicated by the fact that it is proportional to the $\left(\bar{\kappa}^2 - \frac{1}{\Pi}\right)\left[\cosh\bar{\psi} - 1\right]$ and for the present case $\bar{\kappa}^2 \gg 1/\Pi$. This positive pressure gradient would trigger a flow in the direction opposite to that of the direction of the axial temperature gradient (i.e., from the left to right). Or equivalently, this induced pressure-gradient driven TCOS transport will oppose (or favor) the EOS transport generated by the induced positive (negative) electric field (see Fig. 3.2).

Under these generic conditions, we investigate the TOS flows for both brush-grafted and brush-free nanochannels. We start with the case of $c_\infty = 0.0001\ M$, $\alpha = 0$, $\beta = 0$. For these parameter values, the electric field for both brush-free and brush-grafted nanochannels is very weak (see Fig. 3.2). As a consequence the induced EOS transport is very weak (see Fig. 3.3), and the overall TOS transport is dictated by the TCOS transport, making the TOS velocity field significantly negative. More importantly, the EDL localization effect for the end-charged brushes is witnessed here too, given that the induced pressure gradient is proportional to $\left(\bar{\kappa}^2 - \frac{1}{\Pi}\right)\left[\cosh\bar{\psi} - 1\right]$, i.e., depends on the EDL electrostatic potential $\bar{\psi}$. This localization effect would imply that the effect of the pressure gradient, which is localized at the non-grafted end of the brushes (i.e., away from the nanochannel walls), would be more severe as compared to the brush-free nanochannels. On the other hand, the brush-grafted nanochannels

encounter a larger drag force due to the presence of the brushes. These two factors compete with each other. For the weakly grafted brushes, the effect of the localization of the induced pressure-gradient overweighs the enhanced drag; as a consequence, the magnitude of the negative velocity is much larger for the brush-grafted nanochannels as compared to the brush-free nanochannels [compare Fig. 3.3(a) and 3.3(c)]. On the other hand, for the densely grafted brushes the drag force is so large that it outweighs the localization effect leading to a weaker velocity field for the brush-grafted nanochannels [compare Fig. 3.3(b) and 3.3(c)].

We next consider the case for a larger c_∞, i.e., $c_\infty = 0.01\ M$, $\alpha = 0$, $\beta = 0$ (see Fig. 3.4). Here the effect of the TCOS is significantly reduced, implying that for both the brush-free and brush-grafted nanochannels, the TOS transport is very close to the EOS transport. Most importantly, here the localization effect gets severely magnified for the end-charged brushes. A thinner EDL would imply that the EDL cloud extends to much lesser distance around the non-grafted charged end leading to a much stronger localization of the EDL as compared to that for $c_\infty = 0.0001\ M$. On the other hand, a larger c_∞ implies a smaller value of ψ. These two mutually opposing effects interplay with each other to decide the exact extent of the EDL localization effect, which in turn competes with the augmented drag force imparted by the brushes. These factors eventually ensure (a) the magnitude of the velocity for both brush-free and brush-grafted nanochannels is much lower as compared to the cases for $c_\infty = 0.0001\ M$ (see Fig. 3.3), (b) for the nanochannels with the weakly-grafted end charged brushes, the TOS transport is more than one order of magnitude larger than the transport in brush-free nanochannels, and (c) the TOS transport even

for nanochannels with the densely-grafted end charged brushes is larger than that in the brush-free nanochannels.

We next consider the case for a finite, positive α, which leads to a significantly large electric field (or Seebeck coefficient) (see Fig. 3.5). As a result, the EOS flow is large and positive, and hence the TCOS velocity component opposes the EOS transport ensuring a net TOS velocity field whose magnitude is lesser than the EOS flow. This is true for the both the brush-free and the brush-grafted nanochannels. Here both the EOS transport as well as the induced pressure-gradient (and the resultant TCOS transport that opposes the EOS transport) get enhanced for the weakly grafted end-charged brushes. This is evident from the fact that the EOS velocity as well as the extent of decrease in the overall TOC velocity (due to the TCOS velocity) is more for the nanochannels with the weakly-grafted end-charged brushes as compared to the brush-free nanochannels. Of course, the final TOS velocity for the nanochannels with the end-charged brushes remain larger as compared to the brush-free nanochannels. On the other hand, for densely grafted end-charged brushes, the EOS transport as well as the overall TOS transport are distinctly smaller as compared to the brush-free nanochannels.

In Fig. 3.6, we report the same velocity profiles as Fig. 3.5, but for a larger salt concentration ($c_\infty = 0.01\ M$), which ensure (a) the magnitude of the velocity for both brush-free and brush-grafted nanochannels is much lower as compared to the cases for $c_\infty = 0.0001\ M$ (see Fig. 3.5), (b) for the nanochannels with the weakly-grafted end charged brushes, the TOS transport is more than one order of magnitude larger than the transport in brush-free nanochannels, and (c) the TOS transport even for

nanochannels with the densely-grafted end charged brushes is larger than that in the brush-free nanochannels.

In Fig. 3.7, we report the velocity profiles for a negative α, which led to a negative electric field (see Fig. 3.2) and hence a negative EOS velocity. Therefore, the TCOS transport augments the magnitude (negative) of the velocity field. Everything else is very much similar to Fig. 3.5: the EDL localization induced enhancement of the velocity field in nanochannels with less densely grafted brushes leads to a larger magnitude of TOS transport as compared to the brush free nanochannels, while the nanochannels with densely grafted brushes show a weaker velocity (as compared to the brsuh-free nanochannels) due to an augmented drag force.

In Fig. 3.8, we report the same velocity profiles as Fig. 3.7, but for a larger c_∞ ($c_\infty = 0.01\ M$). Exactly the same effect as Fig. 3.6 is witnessed here – the increase of the extent of the EDL localization as well as weaker ψ leads to (a) the magnitude of the velocity for both brush-free and brush-grafted nanochannels is much lower as compared to the cases for $c_\infty = 0.0001\ M$ (see Fig. 3.7), (b) for the nanochannels with the weakly-grafted end charged brushes, the TOS transport is more than one order of magnitude larger than the transport in brush-free nanochannels, and (c) the TOS transport even for nanochannels with the densely-grafted end charged brushes is larger than that in the brush-free nanochannels.

In Fig. 3.9, we consider the case of $\beta > 0$. It has the same influence as that for $\alpha < 0$, i.e., it leads to a large negative electric field. As a result, we witness that (a) the EOS flow is negative, (b) the magnitude of the overall TOS transport increases with the contribution of the TCOS transport, and (c) the nanochannels

with less (more) densely grafted brushes show an increase (decrease) in the overall TOS transport as compared to the brush-free nanochannels.

In Fig. 3.10, we report the same velocity profiles as Fig. 3.9, but for a larger c_∞ ($c_\infty = 0.01\ M$). Exactly the same effect as Fig. 3.8 is witnessed here – (a) the magnitude of the velocity for both brush-free and brush-grafted nanochannels is much lower as compared to the cases for $c_\infty = 0.0001\ M$ (see Fig. 3.9), (b) for the nanochannels with the weakly-grafted end charged brushes, the TOS transport is more than one order of magnitude larger than the transport in brush-free nanochannels, and (c) the TOS transport even for nanochannels with the densely-grafted end charged brushes is larger than that in the brush-free nanochannels.

In Fig. 3.11, we report the velocity profile for $\beta > 0$ and $\alpha > 0$. These two effects counter each other leading to small electric field. Therefore, the result is very similar to that reported in Fig. 3.3: (a) the EOS flow strength is very weak, (b) the TOS transport is dominated by the TCOS transport making the TOS flow profiles negative, (c) the EDL localization affects the pressure gradient making the nanochannels with less densely grafted brushes demonstrate a larger magnitude of the TOS velocity as compared to the brush-free nanochannels, and (d) the drag force in nanochannels with densely grafted brushes ensure that the TOS transport is weaker as compared to that in the brush-free nanochannels.

We next consider the case for a larger c_∞, i.e., $c_\infty = 0.01\ M$, $\alpha = 0.5$, $\beta = 0.5$ (see Fig. 3.12). We witness that (a) the magnitude of the velocity for both brush-free and brush-grafted nanochannels is much lower as compared to the cases for $c_\infty = 0.0001\ M$ (see Fig. 3.11), (b) for the nanochannels with the weakly-grafted

end charged brushes, the TOS transport is more than one order of magnitude larger than the transport in brush-free nanochannels, and (c) the TOS transport even for nanochannels with the densely-grafted end charged brushes is larger than that in the brush-free nanochannels.

In Fig. 3.13, we report the velocity profile for $\beta > 0$ and $\alpha < 0$. Both these factors contribute to make the electric field negative (see Fig. 3.2). Hence we witness a large negative EOS transport, which is augmented further by the TCOS transport to ensure an even larger negative TOS transport. The EDL localization affects makes the nanochannels with less densely grafted brushes demonstrate a larger magnitude of the TOS velocity as compared to the brush-free nanochannels, while the overwhelming influence of the drag force in nanochannels with densely grafted brushes ensure that the TOS transport is weaker as compared to that in the brush-free nanochannels.

In Fig. 3.14, we repeat the same velocity profiles as Fig. 3.13 but for $c_\infty = 0.01$. Enhanced localization as well as reduced $\bar{\psi}$ is ensured for thinner EDLs (or larger c_∞) ensuring (a) the magnitude of the velocity for both brush-free and brush-grafted nanochannels is much lower as compared to the cases for $c_\infty = 0.0001\ M$ (see Fig. 3.13), (b) for the nanochannels with the weakly-grafted end charged brushes, the TOS transport is more than one order of magnitude larger than the transport in brush-free nanochannels, and (c) the TOS transport even for nanochannels with the densely-grafted end charged brushes is larger than that in the brush-free nanochannels.

In Fig. 3.15, we consider the case of $\beta < 0$. This leads to a positive electric field (see Fig. 3.2) causing a large positive EOS transport, which is retarded by the opposing TCOS transport. This is true for the both the brush-free and the brush-

grafted nanochannels. Here both the EOS transport as well as the induced pressure-gradient (and the resultant TCOS transport that opposes the EOS transport) get enhanced for the weakly grafted end-charged brushes due to the dominating influence of the EDL localization. This is evident from the fact that the EOS velocity as well as the extent of decrease in the overall TOC velocity (due to the TCOS velocity) is more for the nanochannels with the weakly-grafted end-charged brushes as compared to the brush-free nanochannels. Of course, the final TOS velocity for the nanochannels with the end-charged brushes remain larger as compared to the brush-free nanochannels. On the other hand, for densely grafted end-charged brushes, the EOS transport as well as the overall TOS transport are distinctly smaller as compared to the brush-free nanochannels.

In Fig. 3.16, we repeat the same velocity profiles as Fig. 3.15 but for $c_\infty = 0.01$. Enhanced localization is ensured for thinner EDLs (or larger c_∞). This along with a reduced $\bar{\psi}$ ensures (a) the magnitude of the velocity for both brush-free and brush-grafted nanochannels is much lower as compared to the cases for $c_\infty = 0.0001\ M$ (see Fig. 3.15), (b) for the nanochannels with the weakly-grafted end charged brushes, the TOS transport is more than one order of magnitude larger than the transport in brush-free nanochannels, and (c) the TOS transport even for nanochannels with the densely-grafted end charged brushes is larger than that in the brush-free nanochannels.

In Fig. 3.17, we consider the TOS velocity profiles for $\alpha > 0$ and $\beta < 0$. These two conditions together ensure a large electric field (see Fig. 3.2) causing a very large positive EOS transport, which is retarded by the TCOS transport making the overall TOS transport weaker than the EOS transport. Here too the nanochannel grafted

with loosely grafted end-charged PE brushes will demonstrate an enhancement of the EOS transport in comparison to the brush-free nanochannels.

In Fig. 3.18, we repeat the same plot as Fig. 3.17 but with a significantly larger c_∞ ($c_\infty = 0.01\ M$) ensuring (a) the magnitude of the velocity for both brush-free and brush-grafted nanochannels is much lower as compared to the cases for $c_\infty = 0.0001\ M$ (see Fig. 3.17), (b) for the nanochannels with the weakly-grafted end charged brushes, the TOS transport is more than one order of magnitude larger than the transport in brush-free nanochannels, and (c) the TOS transport even for nanochannels with the densely-grafted end charged brushes is larger than that in the brush-free nanochannels.

In Fig. 3.19, we report the velocity profile for $\beta < 0$ and $\alpha < 0$. These two effects counter each other leading to small electric field. Therefore, the result is very similar to that reported in Fig. 3.3: (a) the EOS flow strength is very weak, (b) the TOS transport is dominated by the TCOS transport making the TOS flow profiles negative, (c) the EDL localization affects the pressure gradient making the nanochannels with less densely grafted brushes demonstrate a larger magnitude of the TOS velocity as compared to the brush-free nanochannels, and (d) the dominant influence of the drag force in nanochannels with densely grafted brushes ensure that the TOS transport is weaker as compared to that in the brush-free nanochannels.

Finally in Fig. 3.20, we repeat the same plot as Fig. 3.19 but with a significantly larger c_∞ ($c_\infty = 0.01\ M$) ensuring (a) the magnitude of the velocity for both brush-free and brush-grafted nanochannels is much lower as compared to the cases for $c_\infty = 0.0001\ M$ (see Fig. 3.19), (b) for the nanochannels with the weakly-grafted

end charged brushes, the TOS transport is more than one order of magnitude larger than the transport in brush-free nanochannels, and (c) the TOS transport even for nanochannels with the densely-grafted end charged brushes is larger than that in the brush-free nanochannels.

3.4 Conclusions

In this chapter, we provide a detailed analysis of the Seebeck effect and the resultant TOS transport in brush0grafted and brush-free nanochannels in presence of an externally imposed axial positive temperature gradient. Most remarkably we witness that while the Seebeck coefficient (or the thermoosmotically induced electric field) shows very little change due to brush functionalization, the overall strength of the TOS transport can be augmented by more than one order of magnitude for the brush-grafted nanochannels. Such an augmentation occurs for relatively loosely grafted brushes for both positive and negative TOS velocity fields. Such massive extent of augmentation typically occurs at large salt concentration where the effect localization of the EDL away form the nanochannel wall is most severe. In fact for such salt concentrations, the effect of EDL localization can be so influential that the velocity magnitudes even for nanochannels with densely grafted brushes can be more than that in nanochannels without the brushes. Of course, the large concentration would mean a weaker electrostatic potential causing a wekaer magnitude of velocity for both brush-free and brush-grafted nanochannels. Therefore, our study also provides a unique design option of choosing between situations that afford either a more

magnified velocity or a more magnified difference between velocities in brush-grafted and brush-free nanochannels.

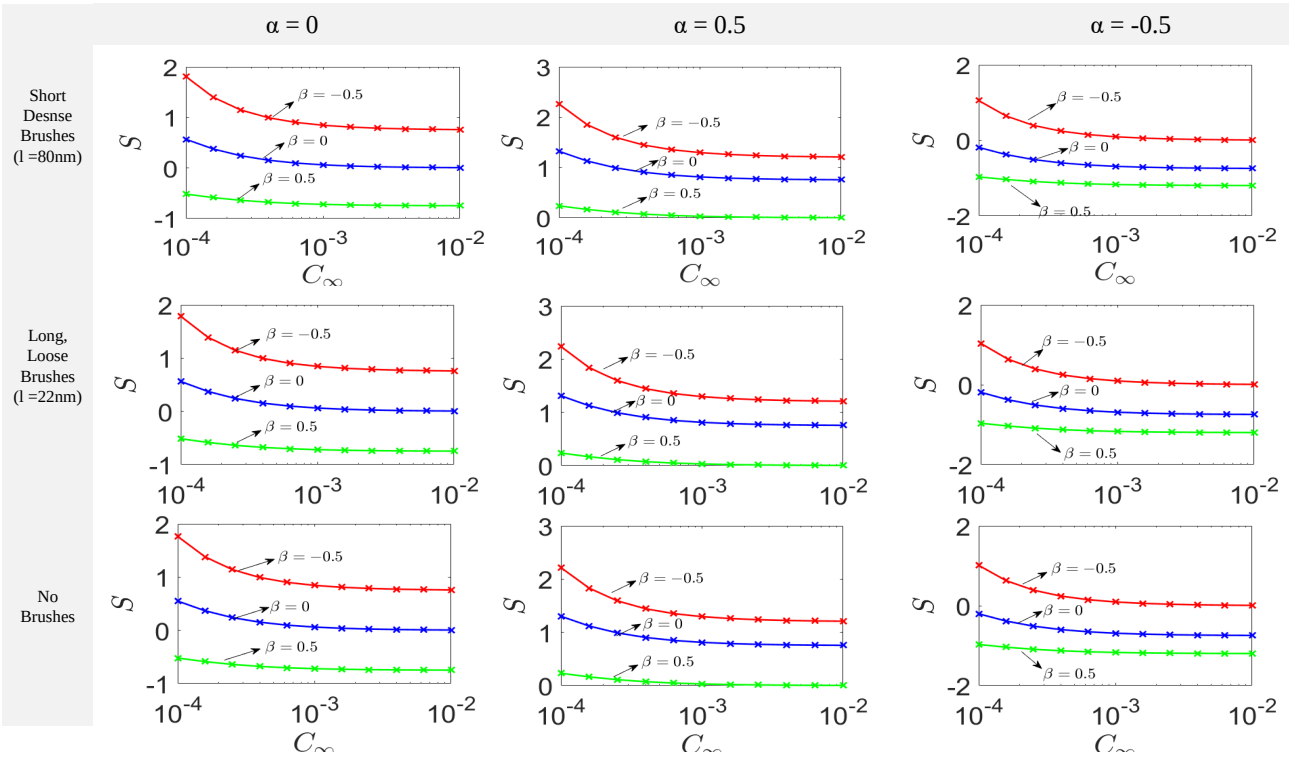

Figure 3.2: Variation of Induced electric field with concentration, β and α for nanochannels with and without brushes. We consider $L\frac{\nabla T_\infty}{T_\infty} = 0.067$, $\frac{\Pi}{T}$ =$5\times10^{-3}K^{-1}$. Other parameters are $\sigma_{ch} = -0.0008C/m^2$ (this charge density is the charge density for brush-free nanochannel walls and the ends of the end-charged PE brushes for nanochannels with PE brushes), $h = 100nm$, $\chi = 0.4$, $a_k = 1nm$, $k_B = 1.38 \times 10^{-23}\ J/K$, $T = 300\ K$, $e = 1.6 \times 10^{-19}C$, $\epsilon_0 = 8.8 \times 10^{-12}F/m$.

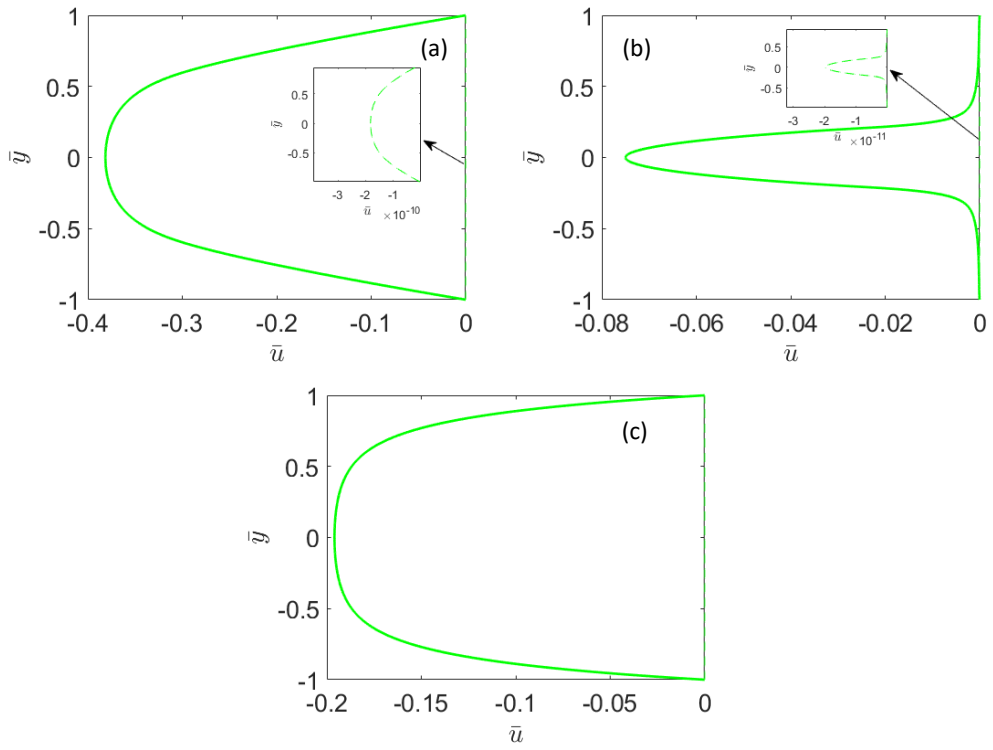

Figure 3.3: Thermo-osmotic velocity (bold lines) and Electro-osmotic velocity (dashed lines) profiles for the case of $C_\infty = 10^{-4}M$, $\alpha = 0$, $\beta = 0$ in (a) Nanochannels grafted with long weakly grafted brushes, (b) Nanochannels grafted with short densely grafted brushes and (c) Nanochannels without brushes. Other parameters are same as those in Fig 2.

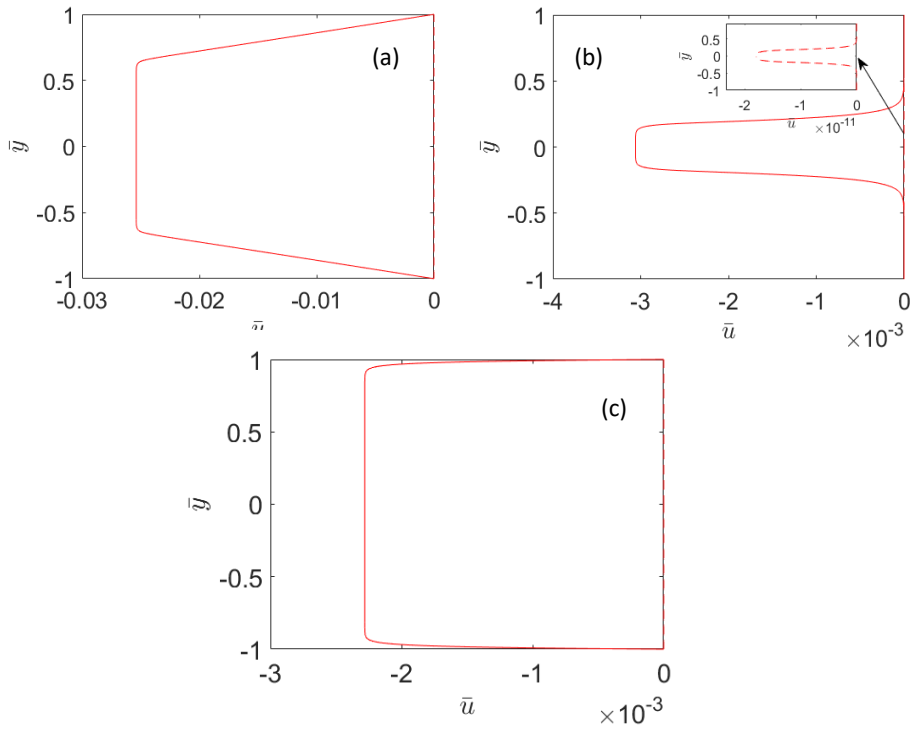

Figure 3.4: Thermo-osmotic velocity (bold lines) and Electro-osmotic velocity (dashed lines) profiles for the case of $C_\infty = 10^{-2}M$, $\alpha = 0$, $\beta = 0$ in (a) Nanochannels grafted with long weakly grafted brushes, (b) Nanochannels grafted with short densely grafted brushes and (c) Nanochannels without brushes. Other parameters are same as those in Fig 2.

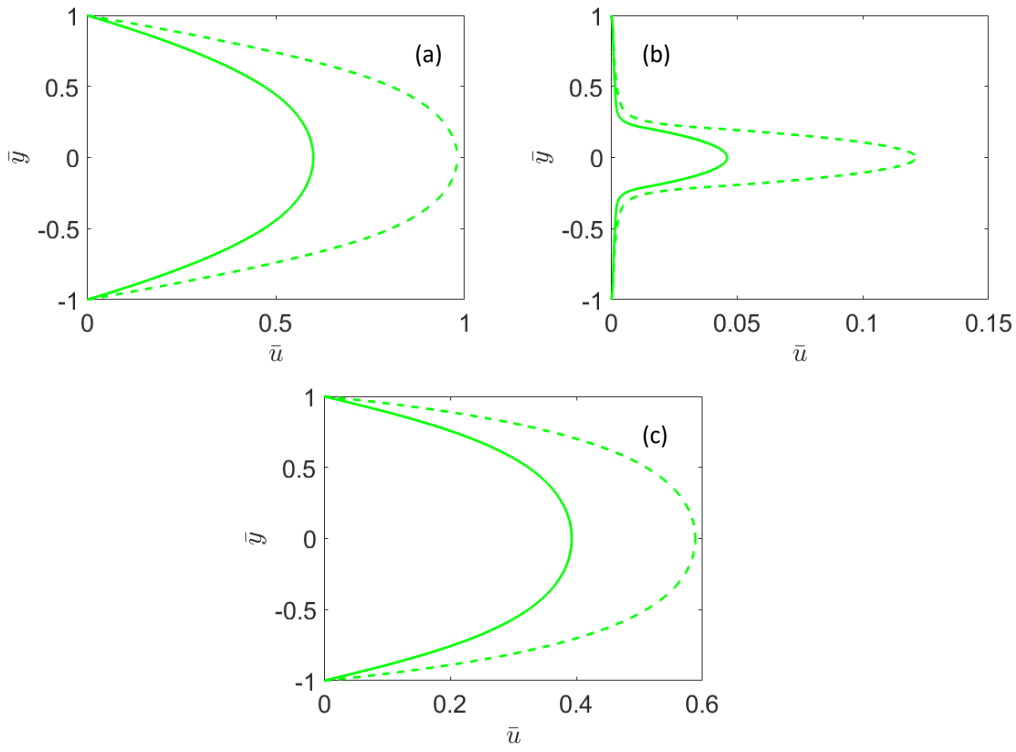

Figure 3.5: Thermo-osmotic velocity (bold lines) and Electro-osmotic velocity (dashed lines) profiles for the case of $C_\infty = 10^{-4}M$, $\alpha = 0.5$, $\beta = 0$ in (a) Nanochannels grafted with long weakly grafted brushes, (b) Nanochannels grafted with short densely grafted brushes and (c) Nanochannels without brushes. Other parameters are same as those in Fig 2.

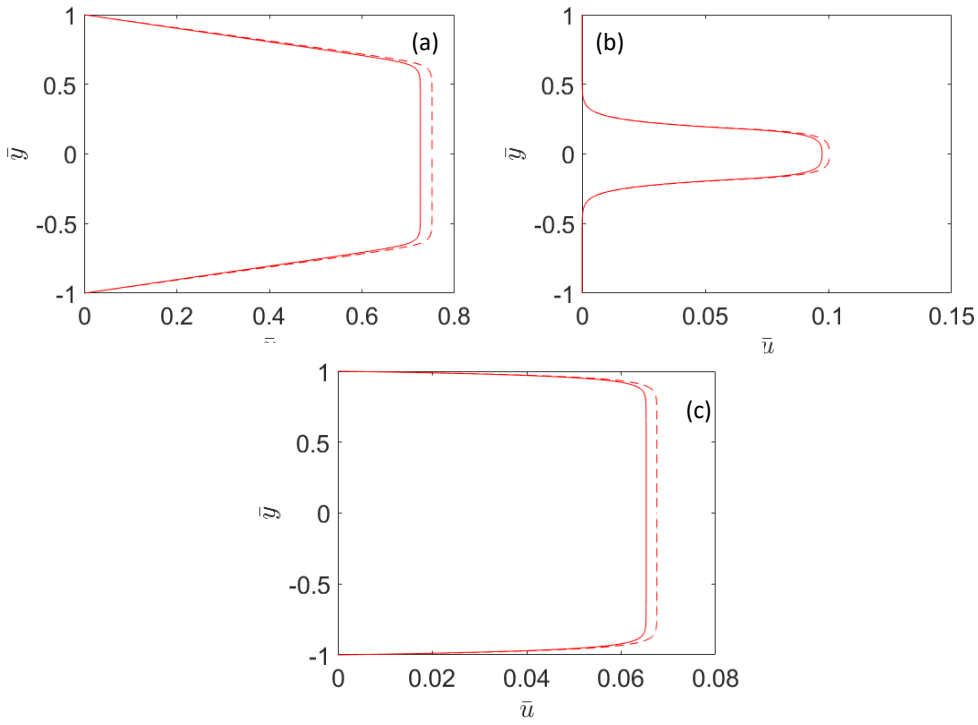

Figure 3.6: Thermo-osmotic velocity (bold lines) and Electro-osmotic velocity (dashed lines) profiles for the case of $C_\infty = 10^{-2}M$, $\alpha = 0.5$, $\beta = 0$ in (a) Nanochannels grafted with long weakly grafted brushes, (b) Nanochannels grafted with short densely grafted brushes and (c) Nanochannels without brushes. Other parameters are same as those in Fig 2.

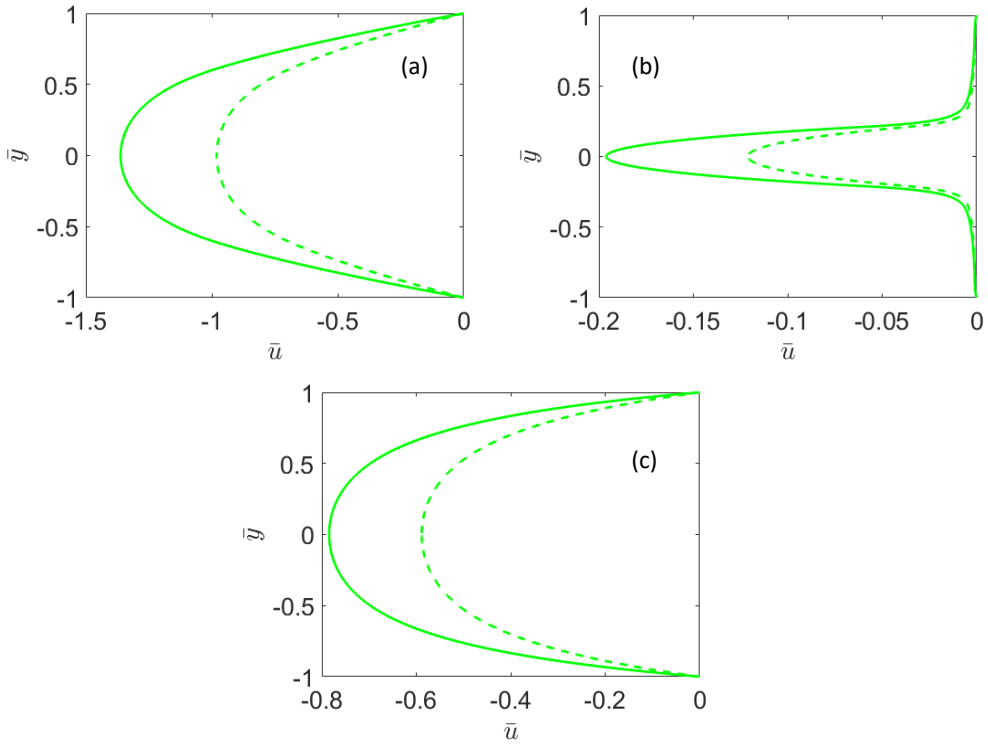

Figure 3.7: Thermo-osmotic velocity (bold lines) and Electro-osmotic velocity (dashed lines) profiles for the case of $C_\infty = 10^{-4}M$, $\alpha = -0.5$, $\beta = 0$ in (a) Nanochannels grafted with long weakly grafted brushes, (b) Nanochannels grafted with short densely grafted brushes and (c) Nanochannels without brushes. Other parameters are same as those in Fig 2.

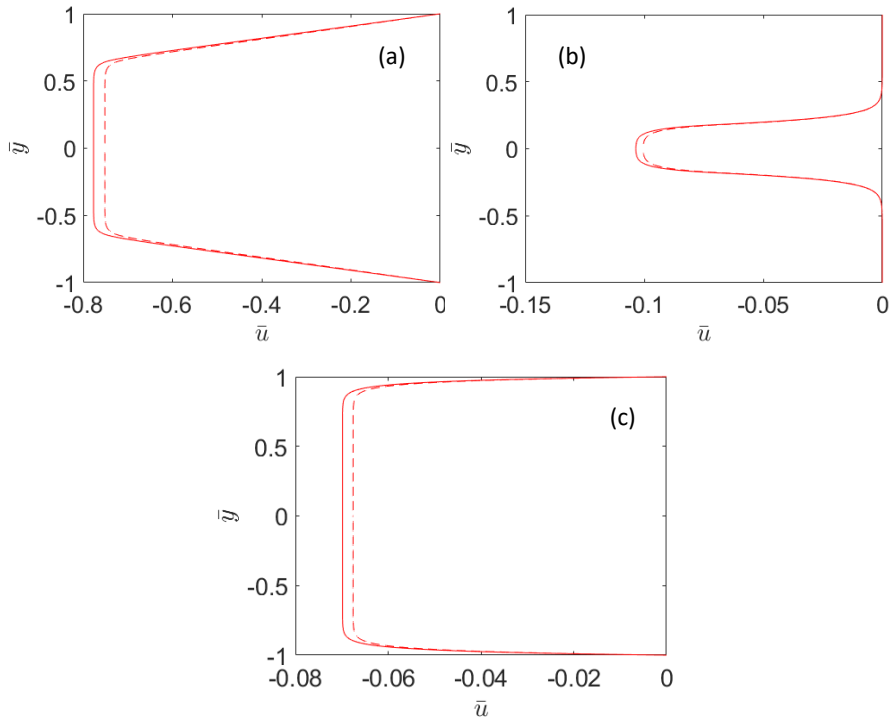

Figure 3.8: Thermo-osmotic velocity (bold lines) and Electro-osmotic velocity (dashed lines) profiles for the case of $C_\infty = 10^{-2}M$, $\alpha = -0.5$, $\beta = 0$ in (a) Nanochannels grafted with long weakly grafted brushes, (b) Nanochannels grafted with short densely grafted brushes and (c) Nanochannels without brushes. Other parameters are same as those in Fig 2.

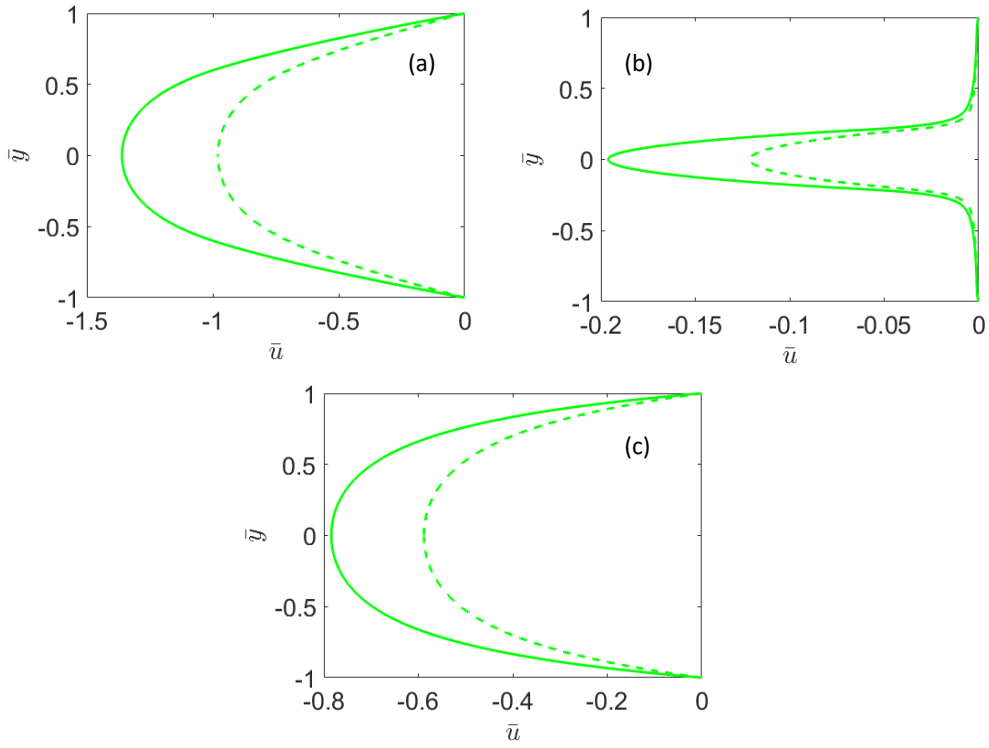

Figure 3.9: Thermo-osmotic velocity (bold lines) and Electro-osmotic velocity (dashed lines) profiles for the case of $C_\infty = 10^{-4}M$, $\alpha = 0$, $\beta = 0.5$ in (a) Nanochannels grafted with long weakly grafted brushes, (b) Nanochannels grafted with short densely grafted brushes and (c) Nanochannels without brushes. Other parameters are same as those in Fig 2.

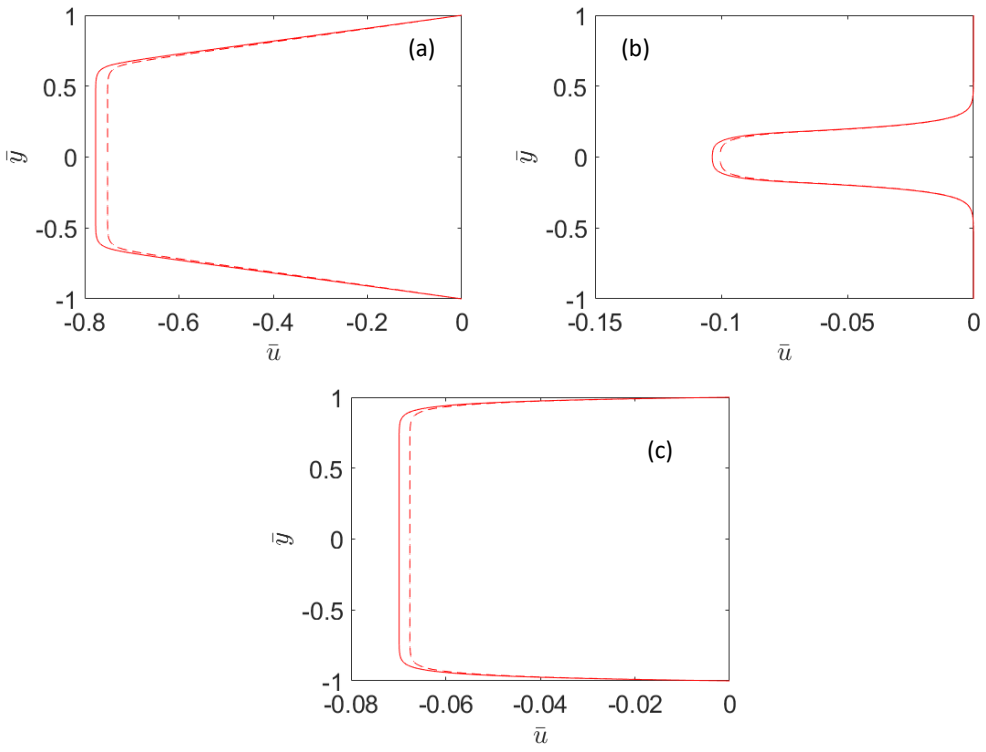

Figure 3.10: Thermo-osmotic velocity (bold lines) and Electro-osmotic velocity (dashed lines) profiles for the case of $C_\infty = 10^{-2}M$, $\alpha = 0$, $\beta = 0.5$ in (a) Nanochannels grafted with long weakly grafted brushes, (b) Nanochannels grafted with short densely grafted brushes and (c) Nanochannels without brushes.

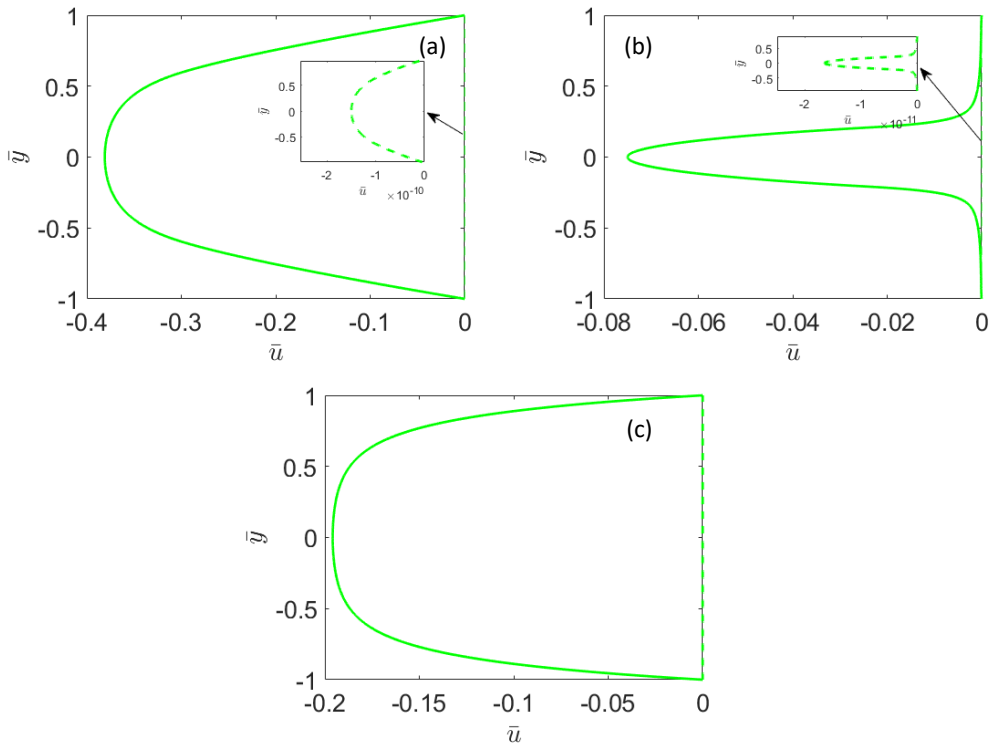

Figure 3.11: Thermo-osmotic velocity (bold lines) and Electro-osmotic velocity (dashed lines) profiles for the case of $C_\infty = 10^{-4}M$, $\alpha = 0.5$, $\beta = 0.5$ in (a) Nanochannels grafted with long weakly grafted brushes, (b) Nanochannels grafted with short densely grafted brushes and (c) Nanochannels without brushes.

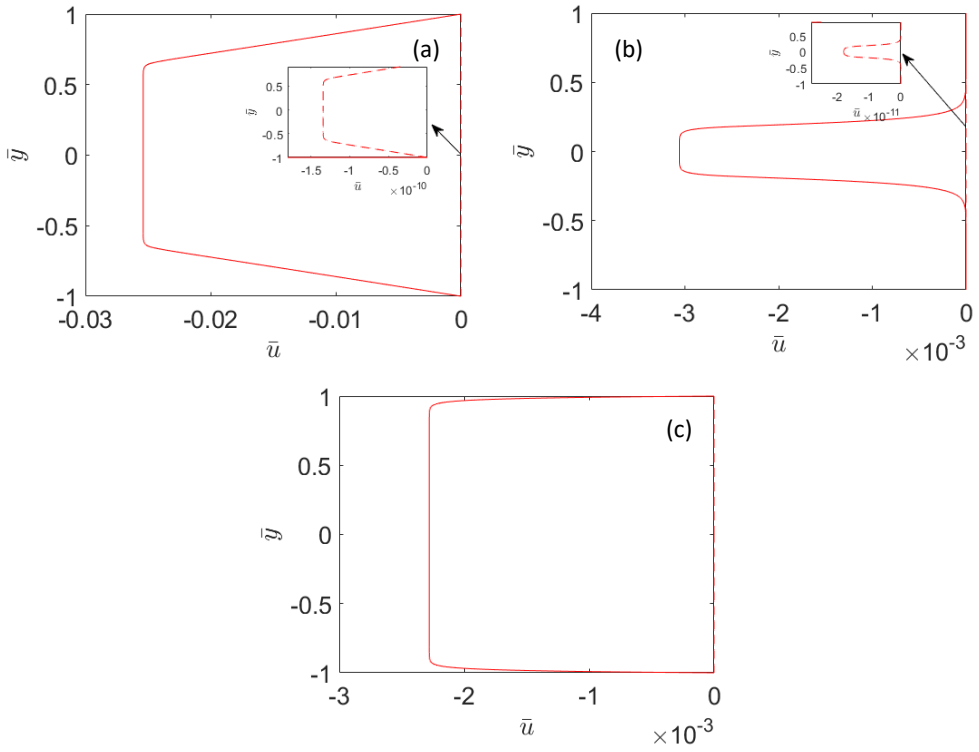

Figure 3.12: Thermo-osmotic velocity (bold lines) and Electro-osmotic velocity (dashed lines) profiles for the case of $C_\infty = 10^{-2}M$, $\alpha = 0.5$, $\beta = 0.5$ in (a) Nanochannels grafted with long weakly grafted brushes, (b) Nanochannels grafted with short densely grafted brushes and (c) Nanochannels without brushes. Other parameters are same as those in Fig 2.

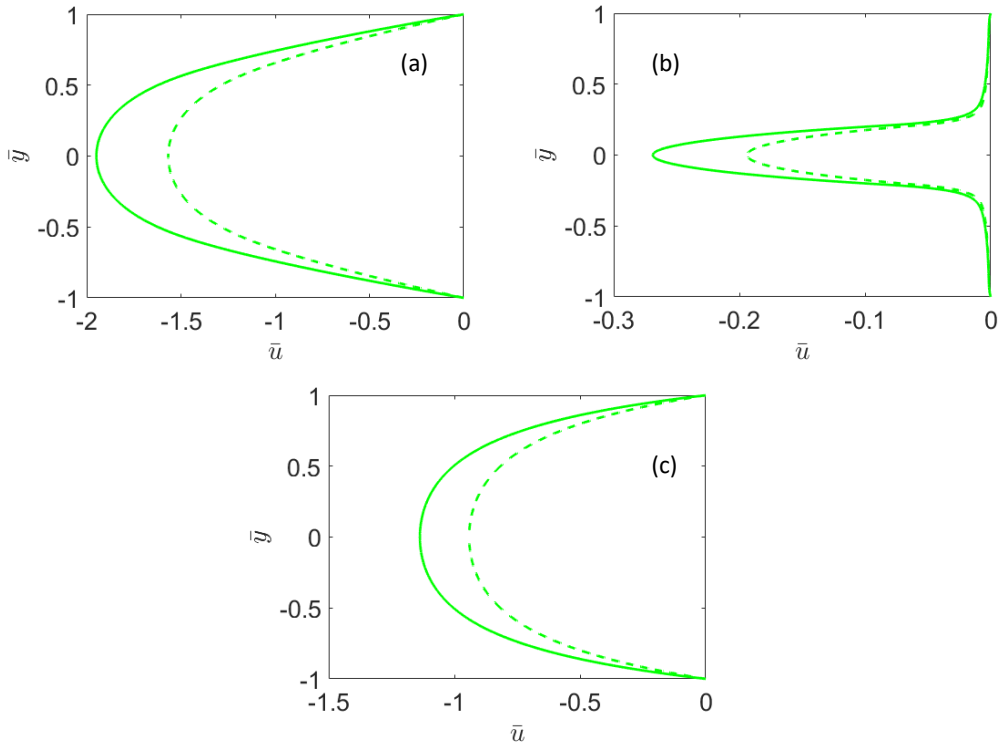

Figure 3.13: Thermo-osmotic velocity (bold lines) and Electro-osmotic velocity (dashed lines) profiles for the case of $C_\infty = 10^{-4}M$, $\alpha = -0.5$, $\beta = 0.5$ in (a) Nanochannels grafted with long weakly grafted brushes, (b) Nanochannels grafted with short densely grafted brushes and (c) Nanochannels without brushes. Other parameters are same as those in Fig 2.

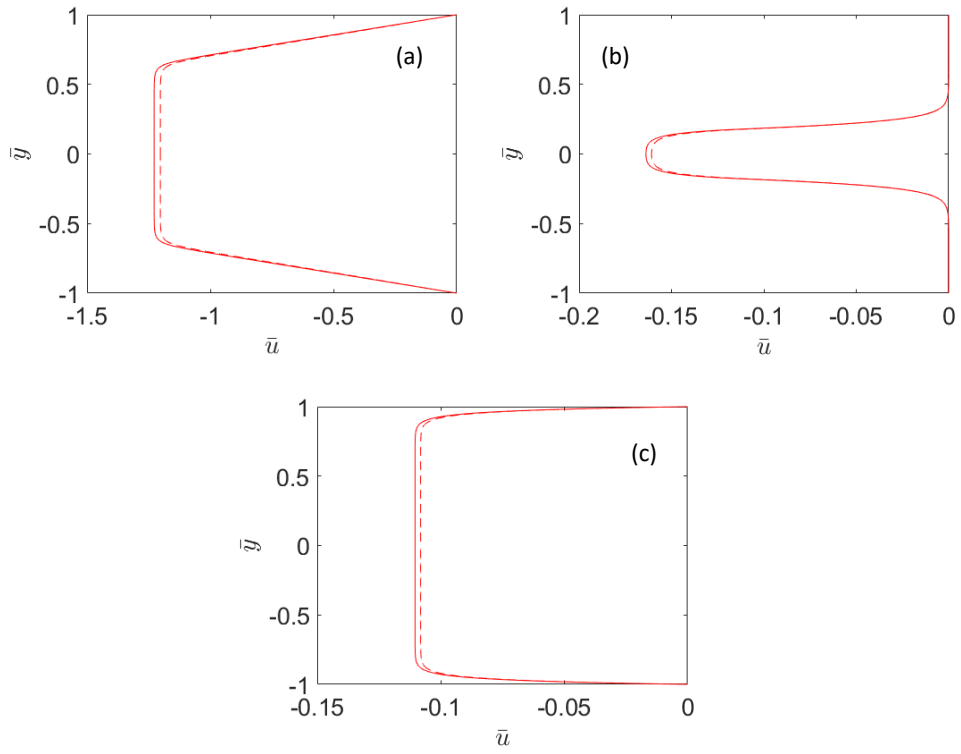

Figure 3.14: Thermo-osmotic velocity (bold lines) and Electro-osmotic velocity (dashed lines) profiles for the case of $C_\infty = 10^{-2}M$, $\alpha = -0.5$, $\beta = 0.5$ in (a) Nanochannels grafted with long weakly grafted brushes, (b) Nanochannels grafted with short densely grafted brushes and (c) Nanochannels without brushes. Other parameters are same as those in Fig 2.

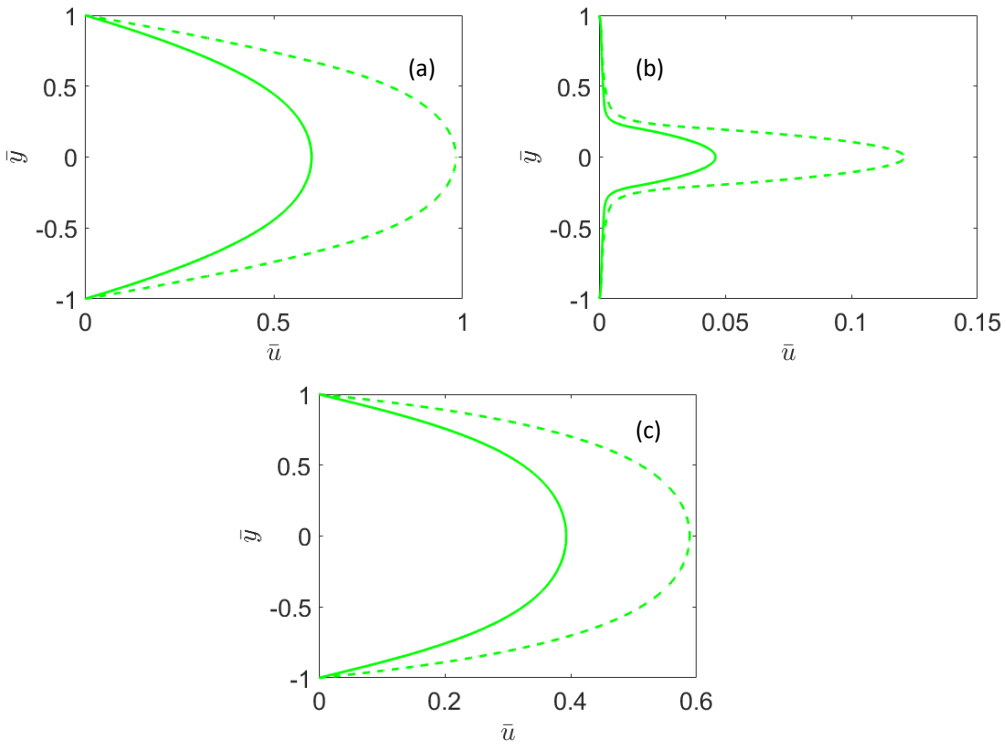

Figure 3.15: Thermo-osmotic velocity (bold lines) and Electro-osmotic velocity (dashed lines) profiles for the case of $C_\infty = 10^{-4}M$, $\alpha = 0$, $\beta = -0.5$ in (a) Nanochannels grafted with long weakly grafted brushes, (b) Nanochannels grafted with short densely grafted brushes and (c) Nanochannels without brushes. Other parameters are same as those in Fig 2.

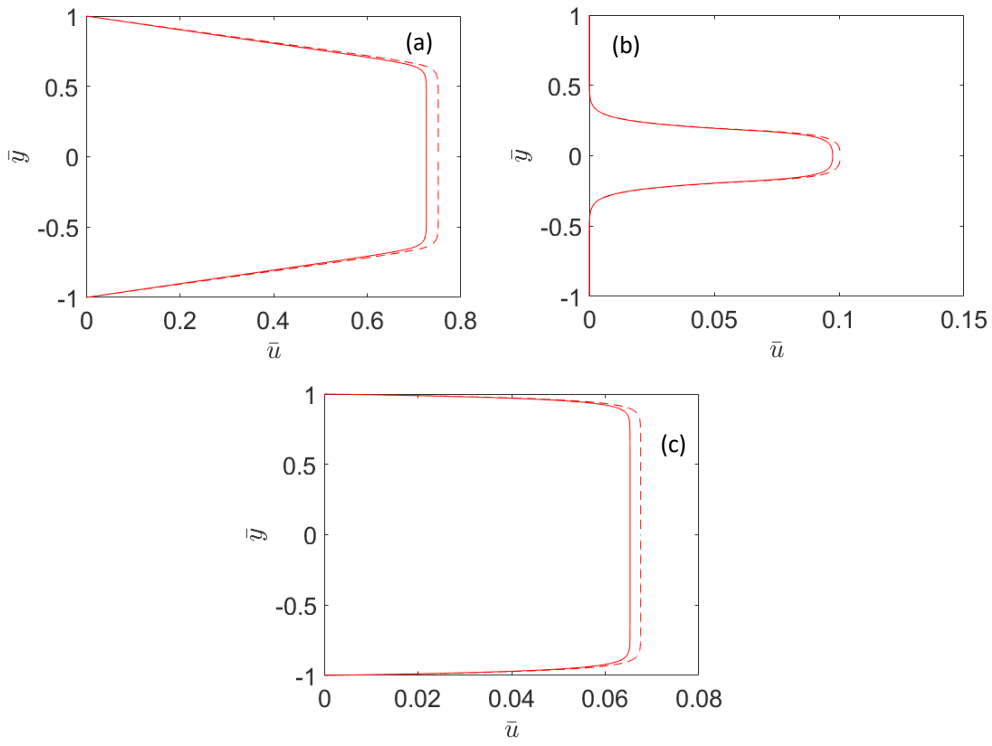

Figure 3.16: Thermo-osmotic velocity (bold lines) and Electro-osmotic velocity (dashed lines) profiles for the case of $C_\infty = 10^{-2}M$, $\alpha = 0$, $\beta = -0.5$ in (a) Nanochannels grafted with long weakly grafted brushes, (b) Nanochannels grafted with short densely grafted brushes and (c) Nanochannels without brushes. Other parameters are same as those in Fig 2.

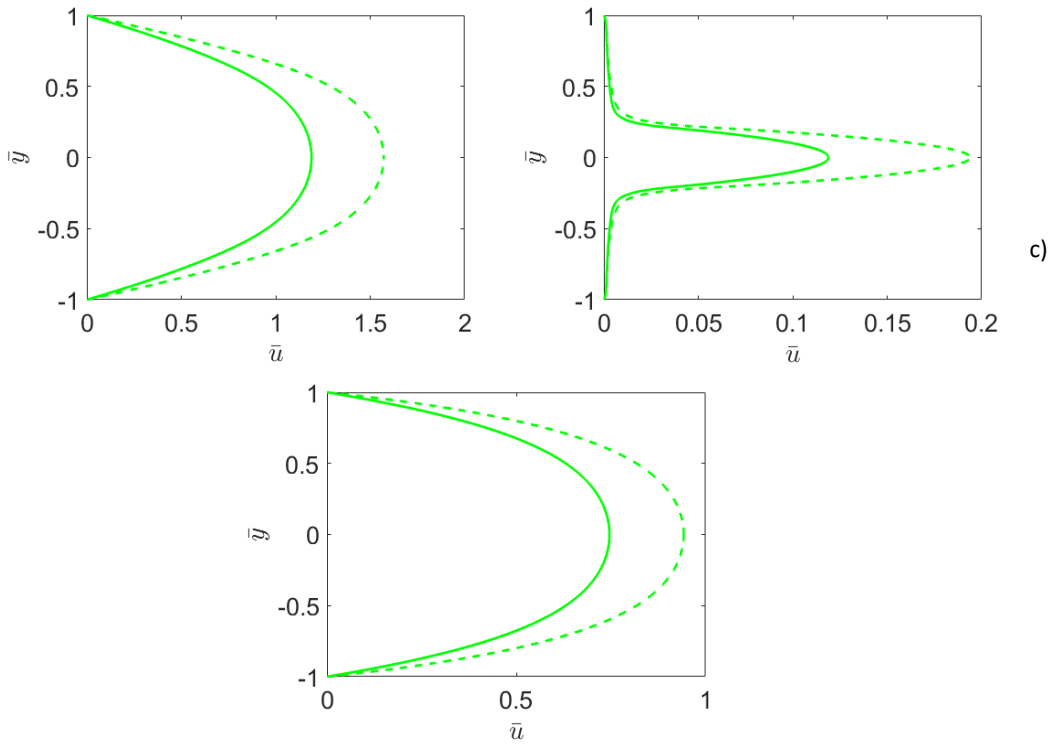

Figure 3.17: Thermo-osmotic velocity (bold lines) and Electro-osmotic velocity (dashed lines) profiles for the case of $C_\infty = 10^{-4}M$, $\alpha = 0.5$, $\beta = -0.5$ in (a) Nanochannels grafted with long weakly grafted brushes, (b) Nanochannels grafted with short densely grafted brushes and (c) Nanochannels without brushes. Other parameters are same as those in Fig 2.

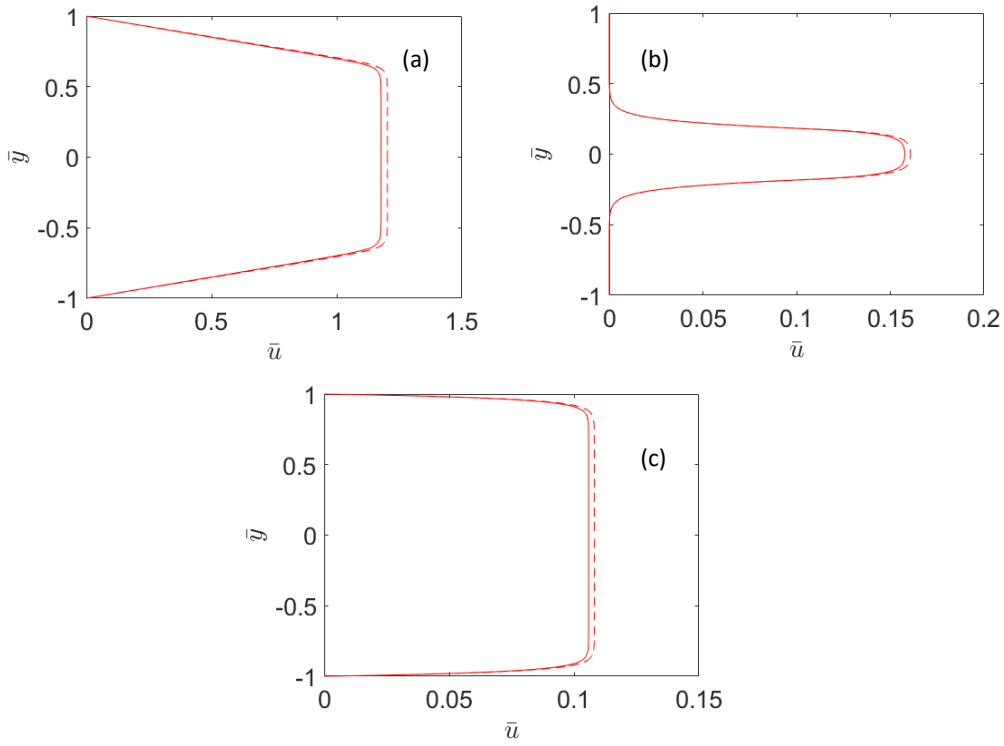

Figure 3.18: Thermo-osmotic velocity (bold lines) and Electro-osmotic velocity (dashed lines) profiles for the case of $C_\infty = 10^{-2}M$, $\alpha = 0.5$, $\beta = -0.5$ in (a) Nanochannels grafted with long weakly grafted brushes, (b) Nanochannels grafted with short densely grafted brushes and (c) Nanochannels without brushes. Other parameters are same as those in Fig 2.

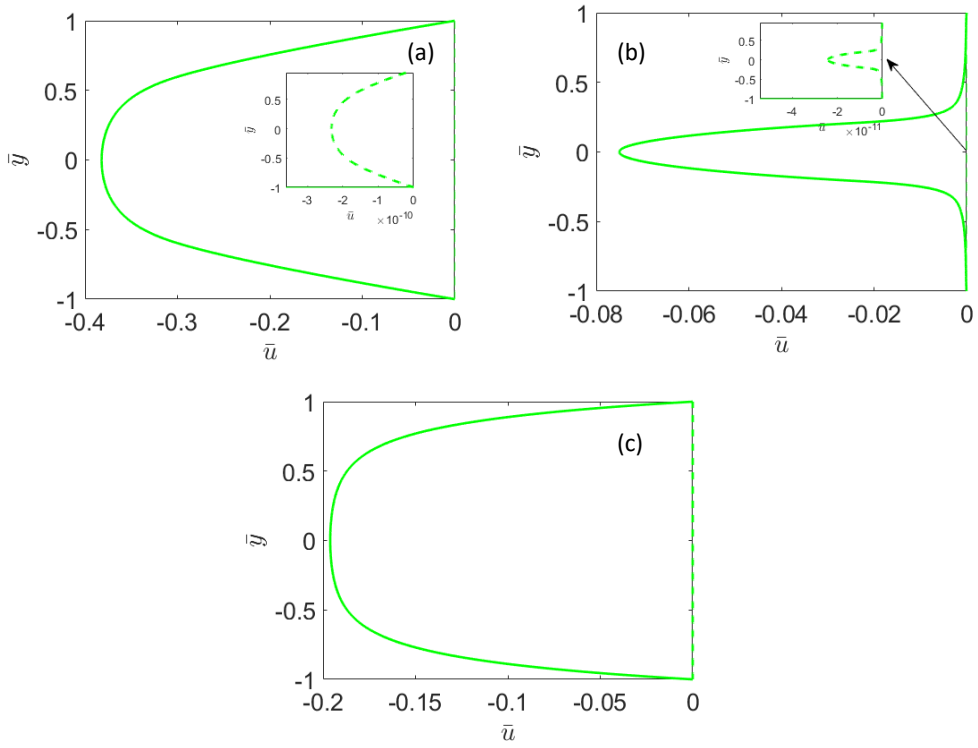

Figure 3.19: Thermo-osmotic velocity (bold lines) and Electro-osmotic velocity (dashed lines) profiles for the case of $C_\infty = 10^{-4}M$, $\alpha = -0.5$, $\beta = -0.5$ in (a) Nanochannels grafted with long weakly grafted brushes, (b) Nanochannels grafted with short densely grafted brushes and (c) Nanochannels without brushes. Other parameters are same as those in Fig 2..

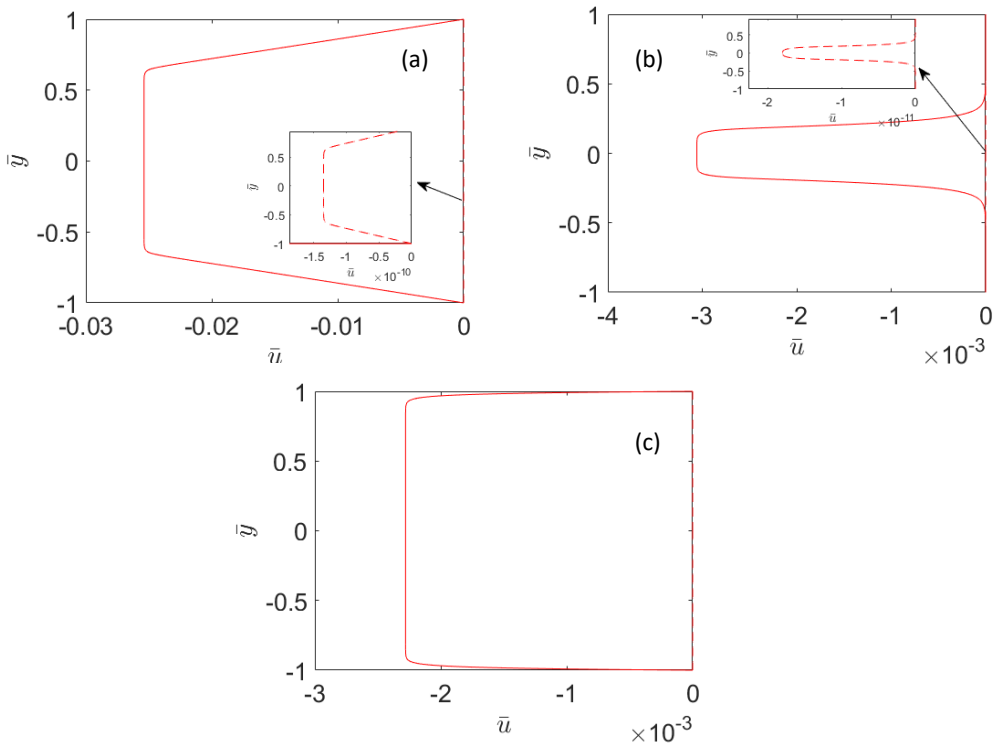

Figure 3.20: Thermo-osmotic velocity (bold lines) and Electro-osmotic velocity (dashed lines) profiles for the case of $C_\infty = 10^{-2}M$, $\alpha = -0.5$, $\beta = -0.5$ in (a) Nanochannels grafted with long weakly grafted brushes, (b) Nanochannels grafted with short densely grafted brushes and (c) Nanochannels without brushes Other parameters are same as those in Fig 2.

Appendix

Derivation of eq. 3.7:

The electric field E is obtained by making the net current equal to zero, i.e.,

$$I = \int_{-h}^{h} (J_+ - J_-). \tag{A1}$$

Here, $J_\pm$ are the cationic and anionic ion fluxes that can be expressed as

$$J_\pm = -D_\pm \left[\nabla n_\pm \pm \frac{e}{k_B T} n_\pm (\Delta\psi - E) + \frac{Q_\pm}{k_B T^2} n_\pm \Delta T \right]. \tag{A2}$$

We use the condition,

$$n_\pm = n_\infty e^{\mp\bar{\psi}} \Rightarrow \nabla n_\pm = \nabla n_\infty e^{\mp\psi} \mp n_\infty e^{\mp\bar{\psi}} \nabla\bar{\psi} = \nabla n_\infty e^{\mp\bar{\psi}} \mp n_\pm \frac{e}{k_B T} \nabla\psi,$$
$$(where \quad \bar{\psi} = \frac{e\psi}{k_B T}). \tag{A3}$$

Therefore,

$$J_\pm = -D_\pm \left[\nabla n_\infty e^{\mp\bar{\psi}} \mp \frac{e}{k_B T} n_\infty e^{\mp\bar{\psi}} E + \frac{Q_\pm}{k_B T^2} n_\infty e^{\mp\bar{\psi}} \nabla T \right] + n_\pm u. \tag{A4}$$

Using eq.(A4) in eq.(A1) as well as expressing $\beta = \frac{D_+ - D_-}{D_+ + D_-}$ and $\alpha = \frac{Q_+ D_+ - Q_- D_-}{Q_+ D_+ - Q_- D_-}$ [so that we can write $D_+ = (\frac{1}{2})(D_+ + D_-)(1+\beta)$ and $D_- = (\frac{1}{2})(D_+ + D_-)(1-\beta)$,$Q_+ D_+ = (\frac{1}{2})(Q_+ D_+ + Q_- D_-)(1+\alpha)$ and $Q_- D_- = (\frac{1}{2})(Q_+ D_+ + Q_- D_-)(1-\alpha)$], we can obtain:

$$\frac{n_\infty}{2k_B T}(D_+ + D_-)(E) \int_{-h}^{h} \left[(1+\beta)e^{-\bar{\psi}} + (1-\beta)e^{\bar{\psi}} \right] dy =$$
$$\int_{-h}^{h} 2u n_\infty sinh(\bar{\psi}) dy + \frac{\nabla n_\infty}{2}(D_+ + D_-) \int_{-h}^{h} \left[(1+\beta)e^{-\bar{\psi}} - (1-\beta)e^{\bar{\psi}} \right] dy +$$
$$\frac{n_\infty \nabla T}{2k_B T^2}(Q_+ D_+ + Q_- D_-) \int_{-h}^{h} \left[(1+\alpha)e^{-\bar{\psi}} + (1-\alpha)e^{\bar{\psi}} \right] dy \tag{A5}$$

$\Longrightarrow$

$$E = \frac{4k_B T}{e(D_+ + D_-)} \frac{\int_{-h}^{h} u sinh(\bar{\psi}) dy}{\int_{-h}^{h} \left[(1+\beta)e^{-\bar{\psi}} + (1-\beta)e^{\bar{\psi}} \right] dy} +$$
$$\frac{k_B T}{e} \frac{\nabla n_\infty}{n_\infty} \frac{\int_{-h}^{h} \left[(1+\beta)e^{-\bar{\psi}} + (1-\beta)e^{\bar{\psi}} \right] dy}{\int_{-h}^{h} \left[(1+\beta)e^{-\bar{\psi}} - (1-\beta)e^{\bar{\psi}} \right] dy} +$$
$$\frac{\nabla T}{eT} \frac{Q_+ D_+ + Q_- D_-}{D_+ - D_-} \frac{\int_{-h}^{h} \left[(1+\alpha)e^{-\bar{\psi}} - (1-\alpha)e^{\bar{\psi}} \right] dy}{\int_{-h}^{h} \left[(1+\alpha)e^{-\bar{\psi}} + (1-\alpha)e^{\bar{\psi}} \right] dy} \tag{A6}$$

$$\Longrightarrow$$

$$\bar{E} = \frac{E}{E_0} =$$

$$\frac{\nabla T}{T}\left\{\frac{-\Pi\left\{\int_{-1}^{1} Pe\sinh\left(\bar{\psi}\right)\bar{u}d\bar{y} + \int_{-1}^{1}\left[\left(1+\beta\right)e^{-\bar{\psi}} - \left(1-\beta\right)e^{\bar{\psi}}\right]d\bar{y}\right\}}{\int_{-1}^{1}\left[\left(1+\beta\right)e^{-\bar{\psi}} + \left(1-\beta\right)e^{\bar{\psi}}\right]d\bar{y}}\right\} +$$

$$\frac{\nabla T}{T}\left\{\frac{\Gamma\int_{-1}^{1}\left[\left(1+\alpha\right)e^{-\bar{\psi}} - \left(1-\alpha\right)e^{\bar{\psi}}\right]d\bar{y}}{\int_{-1}^{1}\left[\left(1+\beta\right)e^{-\bar{\psi}} + \left(1-\beta\right)e^{\bar{\psi}}\right]d\bar{y}}\right\}, \tag{A7}$$

where $\frac{\nabla n_\infty}{n_\infty} = -\Gamma\frac{\nabla T}{T}$ and the other different dimensionless groups are expressed in the main text.

Calculation of u:

The velocity field can be obtained by solving the Navier Stokes under hte conditions that the flow is steady, fully developed and hence uni-directional (in the axial direction):

$$\frac{\partial p}{\partial y} + e(n_+ - n_-)\frac{\partial \psi}{\partial y} = 0, \tag{B1}$$

$$\eta\frac{d^2u}{dy^2} = \frac{\partial p}{\partial x} - e(n_+ - n_-)\left(E - \frac{\partial \psi}{\partial x}\right), \tag{B2}$$

where η is the dynamic viscosity and κ is the inverse of the screening length. Using $n_\pm = n_\infty e^{\mp\bar{\psi}}$, we can re-write the equation as:

$$\frac{\partial p}{\partial y} = 2en_\infty sinh(\bar{\psi})\frac{\partial \psi}{\partial y} = 2n_\infty k_B T sinh(\bar{\psi})\frac{\partial \bar{\psi}}{\partial y}. \tag{B3}$$

Integration the equation with respect to y under the condition that when $p = p_{atm}$ (without any applied pressure gradient) and $\bar{\psi} = 0$, we can write:

$$p = p_{atm} + 2n_\infty k_B T[cosh(\bar{\psi}) - 1]. \tag{B4}$$

Of course from eq.(B4), we can obtain (here ∇ implies $\frac{\partial}{\partial x}$):

$$\frac{\partial p}{\partial x} = 2[cosh(\bar{\psi}) - 1][(\nabla n_\infty)k_B T + n_\infty k_B T \nabla T] + 2n_\infty k_B T sinh(\bar{\psi})\nabla\bar{\psi}. \tag{B5}$$

Consequently, we can reduce eq.(B2) to:

$$\eta\frac{d^2u}{dy^2} = 2[(\nabla n_\infty)k_B T + n_\infty k_B \nabla T] + 2n_\infty k_B T sinh(\bar{\psi})\nabla\bar{\psi}. \tag{B6}$$

Considering $\bar{u} = \frac{u}{U^*}$ and $\bar{y} = \frac{y}{h}$, we can write:

$$\eta\frac{d^2u}{dy^2} = \eta\frac{d}{dy}\left(\frac{du}{d\bar{y}}\frac{d\bar{y}}{dy}\right) = \eta\frac{d}{d\bar{y}}\left(U^\star\frac{d\bar{u}}{d\bar{y}}\frac{d\bar{y}}{dy}\right)\frac{d\bar{y}}{dy} = \frac{\eta U^\star\kappa^2}{\bar{\kappa}^2}\frac{d^2\bar{u}}{d\bar{y}^2} = \frac{2k_B T(\nabla n_\infty)}{\bar{\kappa}^2}\frac{d^2\bar{u}}{d\bar{y}^2}, \tag{B7}$$

where $\bar{\kappa} = \kappa h = \frac{1}{\lambda} = \frac{h}{\lambda}$ $[where\ \lambda = \sqrt{\frac{\epsilon_0\epsilon_r k_B T}{2n_\infty^2 e^2}}]$

Using eq.(B7) in eq.(B6), we can write

$$\frac{d^2\bar{u}}{d\bar{y}^2} = \left(\bar{\kappa}^2 + \frac{\nabla T}{T}\frac{n_\infty}{\nabla n_\infty}\right)[\cosh(\bar{\psi}) - 1] + \frac{n_\infty}{\nabla n_\infty}\frac{e}{k_B T}sinh(\bar{\psi})E. \tag{B8}$$

Using eq (3.3) to replace E, we can finally obtain the velocity field within the brushes [1st equation of eq.(3.7)].

Chapter 4: Conclusions and Scope of the Work

4.1 Conclusions

In this work, we have studied the influence of the presence of polyelectrolyte brushes in diffusio-osmotic flow and thermo-osmotic flow. We began with examining the importance and uniqueness of functionalizing nanochannels, which enables fine-tuning of the surface and flow characteristics in the nanochannels. To understand the influence of polyelectrolyte brushes, we first modeled the brush thermodynamics following past approaches towards brush-brush steric interactions, brush-brush electrostatic interactions and finally, brush-EDL electrostatic interactions. We then modeled the physics of the interaction of the brushes with the surrounding electrolyte, taking, among other things, into account the charge de-neutralizing effect of the electrostatic double layer (EDL) that plays a crucial role in nano-scale flows. The difference in diffusivities of the cations and the anions, and in addition, the difference in their heats of transport in the case of thermo-osmosis, results in the induction of an electric field that is partly influenced by the EDL potential. This electric field in turn induces an electro-osmotic (EOS) flow, thus leading to a two-way coupled state of electric field and flow. In addition to electro-osmotic flow, because of the gradient in the number concentrations of the cations and anions, either by way of an applied concentration

gradient (diffusio-osmosis) or an applied temperature gradient (thermo-osmosis) that leads to a Soret-like equilibrium, a pressure gradient results, which then leads to a chemio-osmotic (COS) flow in diffusio-osmosis, and thermochemio-osmotic (TCOS) flow in thermo-osmosis.

We found that in both cases, viz., diffusio-osmosis and thermo-osmosis in nanochannels grafted with polyelectrolyte brushes, the presence of long weakly-grafted brushes typically massively enhances the flow, while the presence of short brushes often has a retarding influence. This comparison is with respect to the flow in ungrafted nanochannels. This is in contradiction with the widely-held view that the presence of the brushes always leads to a reduction in a flow due to brush-drag. It is important to note here that the extent to which the functionalization affects the flow is dependent on whether the chemio-osmotic transport aids or dampens the electro-osmotic flow, with the former leading to a massive enhancement. We hope that this study will bring to light a new mechanism of electrokinetic transport in functionalized nanochannels that can be applied widely in flow-field dependent applications.

4.2 Scope of Work

The present study represents the first attempt to quantify in a thermodynamically self-consistent framework two new mechanisms of induced electrokinetic transport (namely, ionic diffusioosmosis and ionic thermoosmosis) in soft (or PE brush grafted nanochannels). From a pure academic perspective, the work can be extended to include PE brush design that is commonly encountered, namely brushes with

charges along their entire backbone. There have been previous efforts in quantifying electrokinetic transport in such systems (see [33, 42–48]); however, none has considered ionic diffusioosmosis and ionic thermoosmosis. Equally importantly, all these studies never consider a thermodynamic description of the brushes; rather they simply assume a constant, salt-concentration-independent brush height that while calculating the EOS transport. On the other in Chapters 2 and 3 of this thesis, we quantified the EOS transport in a framework that accounts for the brush height in a thermodynamic self-consistent fashion. This same principle of thermodynamic self-constancy with an emphasis of describing the backbone-charged brushes through a rigorous Strong-Stretching-Theory model (see Refs. [9–11, 14, 15]) will allow a description of the induced EOS transport in form of DOS and TOS transport in soft nanochannels in a manner hitherto unknown in the literature. The second important and more long-term scope of this work would be to solve the problem in a framework enriched by the information of the atomistic simulations. Such atomistic simulations would provide a more accurate prediction of parameters such as drag coefficient, heats of transports, etc., under different conditions of imposed concentration and temperature gradients, which in turn can be used in the continuum model describing the induced electrokinetic transport.

Bibliography

[1] S. Alexander, J. Phys., **38**, 977 (1977).

[2] P.-G. de Gennes, J. Phys., **37**, 1443 (1976).

[3] P.-G. de Gennes, Macromolecules, **13**, 1069 (1980).

[4] R. R. Netz and D. Andelman, Phys. Rep. **380**, 1 (2003).

[5] S. T. Milner, Science **251**, 905 (1991).

[6] S. T. Milner, T. A. Witten and M. E. Cates, Europhys. Lett. **5**, 413 (1988).

[7] S. T. Milner, T. A. Witten and M. E. Cates, Macromolecules **21**, 610 (1988).

[8] A. M. Skvortsov, I. V. Pavlushkov, A. A. Gorbunov, Y. B. Zhulina, O. V. Borisov and V. A. Pryamitsyn, J. Polym. Sci., Part B: Polym. Phys. **30**, 1706 (1988).

[9] Y. B. Zhulina, V. A. Pryamitsyn and O. V. Borisov, Pol. Sci. U.S.S.R. **31**, 205 (1989).

[10] E. B. Zhulina, O. Borisov, V. A. Pryamitsyn and T. M. Birshtein, Macromolecules **24**, 140 (1991).

[11] C. M. Wijmans, J. M. H. M. Scheutjens, and E. B. Zhulina, Macromolecules **25**, 2657 (1992).

[12] S. Mishra, S. Varanasi, and P. P. Varanasi, Macromolecules **22**, 4173 (1989).

[13] S. Das, M. Banik, G. Chen, S. Sinha, R. Mukherjee, Soft Matt. **11**, 8550 (2015).

[14] Y. B. Zhulina and O. V. Borisov, J. Chem. Phys. **107**, 5952 (1997).

[15] Y. B. Zhulina and O. V. Borisov, Langmuir **27**, 10615 (2011).

[16] E. B. Zhulina and M. Rubinstein, Soft Matt. **8**, 9376 (2012).

[17] G. Chen and S. Das, RSC Adv. **5**, 4493 (2015).

[18] G. Chen and S. Das, J. Phys. Chem. B **119**, 12714 (2015).

[19] G. Chen and S. Das, J. Phys. Chem. B **120**, 6848 (2016).

[20] T. Kreer, Soft Matt. **12**, 3479 (2016).

[21] P. R. Desai, S. Sinha, and S. Das, Phys. Rev. E **97**, 032503 (2018).

[22] O. H. Kwon, A. Kikuchi, M. Yamato, and T. Okano, Biomaterials **24**, 1223 (2003).

[23] S. Dey, B. Kellam, M. R. Alexander, C. Alexander, F. R. A. J. Rose, J. Mater. Chem. **21**, 6883 (2011).

[24] B. Xin and J. Hao, J. Chem. Soc. Rev. **39**, 769 (2010).

[25] F. Zhou and W. T. S. Huck, Chem Commun. **48**, 5999 (2005).

[26] S. Samanta and J. Locklin, Langmuir **24**, 9558 (2008).

[27] K. Knop, R. Hoogenboom, D. Fischer, and U. S. Schubert, Angew. Chem. Int. Ed. **49**, 6288 (2010).

[28] J. S. Suk, Q. Xu, N. Kim, J. Hanes, and L. M. Ensign, Adv. Drug Deliver. Rev. $doi : 10.1016/j.addr.2015.09.012$ (2015).

[29] H. ShamsiJazeyi, C. A. Miller, M. S. Wong, J. M. Tour, and R. Verduzco, J. Appl. Polym. Sci. **131**, 40576 (2014).

[30] J. O. Zoppe, R. A. Venditti, O. J. Rojas, J. Colloid Interface Sci. **369**, 202 (2012).

[31] G. V. Ramesh, S. Porel, and T. P. Radhakrishnan, Chem. Soc. Rev. **38**, 2646 (2009).

[32] S. P. Adiga and D. W. Brenner, J. Funct. Biomater **3**, 239 (2012).

[33] G. Chen and S. Das, J. Appl. Phys. **117**, 185304 (2012).

[34] G. W. de Groot, M. G. Santonicola, K. Sugihara, T. Zambelli, E. Reimhult, J. Vörös, and G. J. Vancso, ACS Appl. Mater. Interface. **5**, 1400 (2013).

[35] B. Yameen, M. Ali, R. Neumann, W. Ensinger, W. Knoll, and O. Azzaroni, J. Am. Chem. Soc. **131**, 2070 (2009).

[36] M. Ali, B. Yameen, R. Neumann, W. Ensinger, W. Knoll, and O. Azzaroni, J. Am. Chem. Soc. **130**, 16351 (2008).

[37] M. Ali, B. Schiedt, R. Neumann, and W. Ensinger, Macromol. Biosci. **10**, 28 (2010).

[38] S. Umehara, M. Karhanek, R. W. Davis, and Nader Pourmand, Proc. Natl. Acad. Sci. **106**, 4611 (2009).

[39] M. Ali, B. Yameen, J. Cervera, P. Ramirez, R. Neumann, W. Ensinger, W. Knoll, and O. Azzaroni, J. Am. Chem. Soc. **132**, 8338 (2010).

[40] B. Vilozny, A. L. Wollenberg, P. Actis, D. Hwang, B. Singaram, and N. Pourmand, Nanoscale **5**, 9214 (2013).

[41] M. Ali, P. Ramirez, S. Mafe, R. Neumann, and W. Ensinger, ACS Nano **3**, 603 (2009).

[42] S. Chanda, S. Sinha, and S. Das, Soft Matt. **10**, 7558 (2014).

[43] G. Chen and S. Das, J. Colloid Interface Sci. **445**, 357 (2015).

[44] J. Patwary, G. Chen, and S. Das, Microfluid. Nanofluid. **20**, 37 (2016).

[45] A. Poddar, D. Maity, A. Bandopadhyay, and S. Chakraborty, Soft Matt. **12**, 5968 (2016).

[46] Z. Zeng, L. H. Yeh, M. Zhang, and S. Qian, Nanoscale **7**, 17020 (2015).

[47] Z. Milne, L. H. Yeh, T. H. Chou, and S. Qian, J. Phys. Chem. C **118**, 19806 (2014).

[48] L-H. Yeh, M. Zhang, S. Qian, J-P. Hsu, and S. Tseng, J. Phys. Chem. C **116**, 8672 (2012).

[49] G. Chen and S. Das, J. Phys. Chem. B **121**, 2017, 3130-3141.

[50] W. Gao, J.M.Chan and O.C. Farokhzad, Mol. Pharmaceutics **7**, 1913 (2010)

[51] F. Meng, Y. Zhong, R. Cheng, C. Deng and Z. Zhong, Nanomedicine **9**, 487 (2014).

[52] P. Matricardi, C. D. Meo, T. Coviello and F. Alhaique, Expert Opin. Drug Delivery **5**, 417 (2008).

[53] B. Barati, S. J. Johnson, S. McCool, D. W. Green, G. P. Willhite, and J.-T. Liang, J. Appl.Polym. Sci. **126**, 587 (2012).

[54] G. Liu, M. Cai, X. Wang, F. Zhou, and W. Liu, ACS Appl. Mater. Interfaces **6**, 11625 (2014).

[55] Z. Siwy, L. Tron, P. Kohli, L. A. Baker, C. Trautmann, and C. R. Martin, J. Am. Chem. Soc. **127**, 5000 (2005).

[56] G. Xie, W. Tian, L. Wen, K. Xiao, Z. Zhang, Q. Liu, G. Hou, P. Li, Y. Tian, and L. Jiang, Chem. Commun. **51**, 3135 (2015).

[57] M. Ali, M. N. Tahir, Z. Siwy, R. Neumann, W. Tremel, and W. Ensinger, Anal. Chem. **83**, 1673 (2011).

[58] F. Xia, W. Guo, Y. Mao, X. Hou, J. Xue, H. Xia, L. Wang, Y. Song, H. Ji, Q. Ouyang, Y. Wang, and L. Jiang, J. Am. Chem. Soc. **130**, 8345 (2008).

[59] C. Zhou, L. Mei, Y-S. Su, L-H.Yeh, X. Zhang, and S. Qian, Sens. Actuat. B **229**, 305 (2016).

[60] Y. Jian, F. Li, Y. Liu, L. Chang, Q. Liu, and L. Yang, Colloid. Surf. B **156**, 405 (2017).

[61] Z. Milne, L. H. Yeh, T. H. Chou, and S. Qian, J. Phys. Chem. C **118**, 19806 (2015).

[62] L-H. Yeh, M. Zhang, N. Hu, S. W. Joo, S. Qian, and J-P. Hsu, Nanoscale **4**, 5169 (2012).

[63] L-H. Yeh, M. Zhang, N. Hu, S. W. Joo, S. Qian, and J-P. Hsu, Anal. Chem. **84**, 9615 (2012).

[64] L. Benson, L-H. Yeh, T-H. Chou, and S. Qian, Soft Matter **9**, 9767 (2013).

[65] F. Li, Y. Jian, L. Chang, G. Zhao, and L. Yang, Colloid. Surf. B **147**, 234 (2016).

[66] Q. Cao and H. You, Polymers **8**, 438 (2016).

[67] F. Li, Y. Jian, Z. Xie, Y. Liu, and Q. Liu, RSC Adv. **7**, 82 (2017).

[68] Y. Tsori, D. Andelman and J.-F. Joanny, Europhys. Lett. **82**, 46001 (2008).

[69] G. Chen and S. Das, Electrophoresis **38**, 720 (2017).

[70] W. Sparreboom, A. van den Berg, and J. C. T. Eijkel, Nature Nanotech. **4**, 713 (2009).

[71] S. S. Dukhin and B. V. Derjaguin E. Matijevic (Ed.), Surface and Colloid Science, **Vol. 7 (Wiley, New York)** (1974).

[72] D. C. Prieve, J. L. Anderson, J. P. Ebel, and M. E. Lowell, J. Fluid Mech. **148**, 247 (1984).

[73] J. L. Anderson, Annu. Rev. Fluid Mech. **21**, 61 (1989).

[74] H. J. Keh, Curr. Opin. Colloid Interface Sci. **24**, 13 (2016).

[75] H. J. Keh and H. C. Ma, Langmuir **21**, 5461 (2005).

[76] L. Y. Hsu and H. J. Keh, Ind. Eng. Chem. Res. **48**, 2443 (2009).

[77] H. C. Ma and H. J. Keh, J. Colloid Interface Sci. **298**, 476 (2006).

[78] H. C. Ma and H. J. Keh, J. Colloid Interface Sci. **313**, 686 (2007).

[79] S. Qian, B. Das, and X. Luo, J. Colloid Interface Sci. **315**, 721 (2007).

[80] H. J. Keh and H. C. Ma, Colloid. Surf. A **233**, 87 (2004).

[81] V. Hoshyargar, S. N. Ashrazadeh, and A. Sadeghi, Phys. Chem. Chem. Phys. **17**, 29193 (2015).

[82] V. Hoshyargar, S. N. Ashrazadeh, and A. Sadeghi, Electrophoresis **37**, 809 (2016).

[83] H. J. Keh and H. C. Ma, Langmuir **23**, 2879 (2007).

[84] I. Cho, W. Kim, J. Kim, H-Y. Kim, H. Lee, and S. J. Kim, Phys. Rev. Lett. **116**, 254501 (2016).

[85] H. J. Keh and H. C. Ma, Microfluid Nanofluid **5**, 347 (2008).

[86] J. L. Anderson, M. E. Lowell, and D. C. Prieve, J. Fluid Mech. **117**, 107 (1982).

[87] C. Lee, C. Cottin-Bizonne, R. Fulcrand, L. Joly, and C. Ybert, J. Phys. Chem. Lett. **8**, 478 (2017).

[88] M. Shen, F. Ye, R. Liu, K. Chen, M. Yang, and M. Ripoll, J. Chem. Phys. **145**, 124119 (2016).

[89] S. Marbach, H. Yoshida, and L. Bocquet, J. Chem. Phys. **146**, 194701 (2017).

[90] H. Yoshida, S. Marbach, and L. Bocquet, J. Chem. Phys. **146**, 194702 (2017).

[91] A. Ajdari and L. Bocquet, Phys. Rev. Lett. **96**, 186102 (2006).

[92] C. Lee, C. Cottin-Bizonne, A.-L. Biance, P. Joseph, L. Bocquet, and C. Ybert, Phys. Rev. Lett. **112**, 244501 (2014).

[93] I. Ortiz-Riveraa, H. Shumb, A. Agrawal, A. Sen, and A. C. Balazs, Proc. Natl. Acad. Sci. USA **113**, 2585 (2016).

[94] D. Feldmann, S. R. Maduar, M. Santer, N. Lomadze, O. I. Vinogradova, and S. Santer, Sci. Rep.**6**, 36443 (2016).

[95] V. Hoshyargar, S. N. Ashrazadeh, and A. Sadeghi, Phys. Fluid. **29**, 012001 (2017).

[96] T. H. Geballe and G. W. Hull, Phys. Rev. **94**, 1134 (1954).

[97] T. H. Geballe and G. W. Hull, Phys. Rev. **98**, 940 (1955).

[98] K. Uchida, S. Takahashi, K. Harii, J. Ieda, W. Koshibae, K. Ando, S. Maekawa, and E. Saitoh, Nature **455**, 778 (2008).

[99] S. B. Rifaat and X. Ma, Appl. Thermal Eng. **23**, 913 (2003).

[100] D. Zhao and G. Tan, Appl. Thermal Eng. **66**, 15 (2014).

[101] N. S. Hudak and G. G. Amatucci, J. Appl. Phys. **103**, 101301 (2008).

[102] I. Chikina, V. Shikin, and A. A. Varlamov, Phys. Rev. E **86**, 011505 (2012).

[103] W. Kobayashi, A. Kinoshita, and Y. Moritomo, Appl. Phys. Lett. **107**, 073906 (2015).

[104] A. Majee and A. Wrger, Phys. Rev. Lett. **108**, 118301 (2012).

[105] A. Wurger, Phys. Rev. Lett. **101**, 108302 (2008).

[106] A. Wurger, Rep. Prog. Phys. **73**, 126601 (2010).

[107] M. Dietzel and S. Hardt, Phys. Rev. Lett. **116**, 225901 (2016).

[108] M. Dietzel and S. Hardt, J. Fluid Mech. **813**, 1060 (2017).

[109] K. Yanagi et al., Nano Lett. **14**, 6437 (2014).

[110] A. Ly, A. Majee and A. Wurger, New J. Phys. **20**, 025001 (2018).